D E P A R T M E N T O F M A T H E M A T I C S

THE NUMERICAL SOLUTION OF ONE-DIMENSIONAL SHALLOW-WATER PROBLEMS USING THE TAYLOR-GALERKIN METHOD

R. O. MOODY

Numerical Analysis Report no. 8/89

U N I V E R S I T Y O F R E A D I N G

THE NUMERICAL SOLUTION OF

ONE-DIMENSIONAL SHALLOW-WATER PROBLEMS

USING THE TAYLOR-GALERKIN METHOD

R. O. MOODY

Numerical Analysis Report no. 8/89

University of Reading
Mathematics Department
P O Box 220, Whiteknights
Reading, RG6 2AX. U.K.

This work was funded by the Central Electricity Generating Board of England and Wales.

TABLE OF CONTENTS

1. INTRODUCTION

The generation of electrical energy using tidal energy has been shown by H.M.S.O. (1981) to be economically viable, and Count (1980), Wilson *et al.* (1981), Jefferys (1981), and Berry (1982) have conducted extensive investigations into the operation of tidal-power schemes at maximum efficiency.

One such *optimal* approach is that using Optimal Control Theory, which has been incorporated into the numerical algorithms of Birkett and Nichols (1983,1986), Berry, Birkett, Count, and Nichols (1984), Birkett, Count, Nichols, and Nicol (1984), and Birkett (1985,1986). These workers maximise a functional (representing the revenue or average power) subject to the satisfaction of fluid-flow equations in an estuary. They then apply numerical techniques to solve the resulting problem. The optimal-control loop incorporated into the numerical method is the Conditional Gradient Algorithm, which requires the evaluation of derivatives of turbine/sluice-characteristic functions. In certain data, these characteristic functions are discontinuous, and Moody (1989) encountered problems associated with smoothing such data. He concluded that, for such problematic functions, a derivative-free optimal-control loop was required.

The work in this report is a continuation of that by Moody (1989). An intended future task is to incorporate the optimal-control approach of the Reading Group into the two-dimensional finite-element shallow-water

program of the Bristol Group, for the purposes of the CEGB. Now the Bristol Group anticipates difficulties in imposing barrier conditions into its code, so valuable advice in this area may well be gained from the coding of a one-dimensional shallow-water problem using a finite-element method. A finite-element method which has achieved recent success in the numerical solution of fluid-flow problems is the Taylor-Galerkin Method of Donea (1984).

The aim of the work presented in this report is to produce a finite-element code capable of simulating the flow in an estuary. In Section 2 we describe the mathematical formulation of and the numerical method used to solve the shallow-water problem without a barrier, then analyse the numerical results. In Section 3 we introduce a barrier into the problem, and derive an analytic solution for a simplified version. We also describe additional necessary numerical techniques, then present numerical results. Finally, we draw our conclusions and discuss future work in Section 4.

2. THE SHALLOW-WATER PROBLEM WITHOUT A BARRIER

This section contains the work on Problem 1, a one-dimensional shallow-water problem in which there is no barrier. We begin in Subsection 2.1 by describing the mathematical formulation of this simple problem. Subsection 2.2 then consists of a detailed derivation of the Taylor-Galerkin Method of Donea (1984), together with a discussion of other numerical techniques utilised. Subsequently, in Subsection 2.3, we report several simulations and analyse the numerical and graphical results for Problem 1.

2.1 Mathematical Formulation of Problem 1

Suppose that a one-dimensional estuary occupies the region $[0,L]$ in space. Let v denote the fluid flow (i.e., the product of velocity and cross-sectional area) and let η be the elevation above the datum level. Then the linearised shallow-water problem (governing v and η), named Problem 1, is formulated as

$$\left.\begin{aligned} & v_t + g\, a(x)\, \eta_x + p(x)\, v = 0 \\ & b(x)\, \eta_t + v_x = 0 \end{aligned}\right\}, \quad 0 \le x \le L,\ 0 \le t \le T, \tag{2.1}$$

$$\left.\begin{aligned} & v(L,t) = 0 \\ & \eta(0,t) = f(t) \end{aligned}\right\}, \quad 0 \le t \le T, \tag{2.2}$$

$$\left.\begin{aligned} v(x,0) &= v(x,T) \\ \eta(x,0) &= \eta(x,T) \end{aligned}\right\}, \quad 0 \leq x \leq L, \tag{2.3}$$

where g is the acceleration due to gravity and T is the tidal period. The functions a and b are the cross-sectional area and breadth respectively of the estuary, p represents the frictional force, and f denotes the tide function (which is of period T). The boundary conditions are (2.2), and the "initial" conditions, (2.3), ensure a periodic solution for v and η. For simplicity, we take the friction to be

$$p(x) = p_0/h(x), \quad 0 \leq x \leq L, \tag{2.4}$$

in which p_0 is a constant and h determines the depth of the estuary.

2.2 Numerical Techniques Applied to Problem 1

Here we supply a detailed derivation of the Euler-Taylor-Galerkin Method of Donea (1984), as opposed to his other forms of Taylor-Galerkin. The first stage of the method for the flow, v, is as follows. We expand v in a Taylor series to obtain

$$v(x,t+\delta t) = v + \delta t\, v_t + \tfrac{1}{2}(\delta t)^2 v_{tt} + \tfrac{1}{6}(\delta t)^3 v_{ttt} + O[(\delta t)^4], \tag{2.5}$$

where the right-hand side is evaluated at (x,t). Let

$$\left.\begin{aligned} c(x) &= g\, a(x) \\ d(x) &= 1/b(x) \end{aligned}\right\}, \quad 0 \le x \le L, \tag{2.6}$$

then we obtain from Equation (2.1)

$$v_t = - c(x)\, \eta_x - p(x)\, v \tag{2.7}$$

and

$$\eta_t = - d(x)\, v_x, \tag{2.8}$$

for $x \in [0,L]$ and $t \in [0,T]$. Equation (2.7) is an expression for v_t which invloves no time derivatives. We obtain an analagous one for v_{tt} by differentiating (2.7) partially with respect to t and (2.8) with respect to x; i.e.,

$$v_{tt} = - c(x)\, \eta_{xt} - p(x)\, v_t \tag{2.9}$$

and

$$\eta_{xt} = - [d(x)\, v_x]_x. \tag{2.10}$$

Substitution of (2.7) and (2.10) into (2.9) produces

$$v_{tt} = c(x)\, [d(x)\, v_x]_x + p(x)\, c(x)\, \eta_x + [p(x)]^2\, v. \tag{2.11}$$

In order to obtain an analagous form for v_{ttt}, we differentiate (2.11) partially with respect to t, then replace the v_t and η_{xt} terms using (2.7) and (2.10) to give

$$v_{ttt} = c(x)\,[d(x)\,v_{xt}]_x - p(x)\,c(x)\,[d(x)\,v_x]_x -$$

$$[p(x)]^2\,c(x)\,\eta_x - [p(x)]^3\,v. \qquad (2.12)$$

As it is our intention to use piecewise-linear basis functions in space, we cannot eliminate the v_{xt} term in the same way as before, since this act would introduce a v_{xxx} term (which is meaningless when v is piecewise linear). Instead, we include an Euler-type approximation:

$$v_{xt}(x,t) \simeq [v_x(x,t+\delta t) - v_x(x,t)]/\delta t \qquad (2.13)$$

(where δt is an increment in time), which we represent numerically by

$$v^n_{xt} = [v^{n+1}_x - v^n_x]/\delta t, \qquad (2.14)$$

for each time level, n. Hence, substitution of (2.7), (2.11), and (2.12) into (2.5), then discretising and including (2.14), produces

$$v^{n+1} = v^n - \delta t\,\{c(x)\,\eta^n_x + p(x)\,v^n\} + \tfrac{1}{2}\,(\delta t)^2\,\{c(x)\,[d(x)\,v^n_x]_x +$$

$$p(x)\,c(x)\,\eta^n_x + [p(x)]^2\,v^n\} + \tfrac{1}{6}\,(\delta t)^3\,\{c(x)\,(d(x)\,[v^{n+1}_x -$$

$$v^n_x])_x/\delta t - p(x)\,c(x)\,[d(x)\,v^n_x]_x - [p(x)]^2\,c(x)\,\eta^n_x -$$

$$[p(x)]^3 \, v_x^n\}, \tag{2.15}$$

on ignoring the error term. The expression for η, corresponding to (2.15), is

$$\eta^{n+1} = \eta^n - \delta t \, \{d(x) \, v_x^n\} + \tfrac{1}{2} \, (\delta t)^2 \, \{d(x) \, [c(x) \, \eta_x^n]_x +$$

$$d(x) \, [p(x) \, v^n]_x\} + \tfrac{1}{6} \, (\delta t)^3 \, \{d(x) \, (c(x) \, [\eta_x^{n+1} - \eta_x^n])_x/\delta t -$$

$$d(x) \, [p(x) \, c(x) \, \eta_x^n]_x - d(x)[(p(x))^2 \, v]_x\}. \tag{2.16}$$

At this point we have discretised v and η in time only; we now apply the Galerkin finite-element approach using piecewise-linear basis functions. Let x_j, $j = 1(1)N$ be the nodes of a mesh fixed in space. Then we seek approximations $\tilde{v}$ and $\tilde{\eta}$ to v and η respectively, in the form

$$\tilde{v}(x,t) = \sum_{j=1}^{N} v_j(t) \, \alpha_j(x), \tag{2.17}$$

$$\tilde{\eta}(x,t) = \sum_{j=1}^{N} \eta_j(t) \, \alpha_j(x), \tag{2.18}$$

(for $x \in [0,L]$ and $t \in [0,T]$) in which v_j, η_j, $j = 1(1)N$, are unknown amplitudes, and α_j, $j = 1(1)N$, are piecewise-linear basis functions, one of which is depicted in Figure 1.

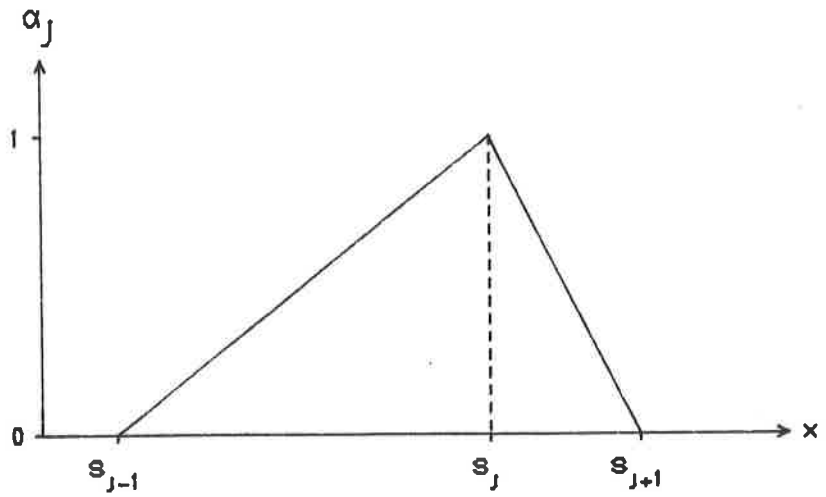

Figure 1

We now (i) take the Galerkin *weak-form* (i.e., multiply by α_i for $i = 1(1)N$ in turn, then integrate over the spatial domain) of (2.15) and (2.16), (ii) replace v and η by $\tilde{v}$ and $\tilde{\eta}$ respectively (using (2.17) and (2.18)), then (iii) apply the usual integration-by-parts technique (to eliminate difficulties associated with second-order spatial derivatives). These operations result in

$$\sum_{j=1}^{N} \{\langle \alpha_i \, , \, \alpha_j \rangle / \delta t + \tfrac{1}{6} \, \delta t \, \langle [c(x) \, \alpha_i]' \, , \, d(x) \, \alpha_j' \rangle\} \, [v_j^{n+1} - v_j^n] =$$

$$\sum_{j=1}^{N} \{- \langle \alpha_i \, , \, p(x) \, \alpha_j \rangle - \tfrac{1}{2} \, \delta t \, \langle [c(x) \, \alpha_i]' \, , \, d(x) \, \alpha_j' \rangle +$$

$$\tfrac{1}{2} \, \delta t \, \langle \alpha_i \, , \, [p(x)]^2 \, \alpha_j \rangle + \tfrac{1}{6} \, (\delta t)^2 \, \langle [p(x) \, c(x) \, \alpha_i]' \, , \, d(x) \, \alpha_j' \rangle -$$

$$\tfrac{1}{6}\,(\delta t)^2\,\langle \alpha_i\ ,\ [p(x)]^3\ \alpha_j\rangle\}\ v_j^n + \sum_{j=1}^{N} \{-\langle \alpha_i\ ,\ c(x)\ \alpha_j'\rangle +$$

$$\tfrac{1}{2}\,\delta t\,\langle \alpha_i\ ,\ p(x)\ c(x)\ \alpha_j'\rangle - \tfrac{1}{6}\,(\delta t)^2\,\langle \alpha_i\ ,\ [p(x)]^2\ c(x)\ \alpha_j'\rangle\}\ \eta_j^n +$$

$$\tfrac{1}{6}\,\delta t\,[c(x)\ d(x)\ (v_x^{n+1} - v_x^n)\ \alpha_i]_{x_1}^{x_N} + \tfrac{1}{2}\,\delta t\,[c(x)\ d(x)\ v_x^n\ \alpha_i]_{x_1}^{x_N} -$$

$$\tfrac{1}{6}\,(\delta t)^2\,[p(x)\ c(x)\ d(x)\ v_x^n\ \alpha_i]_{x_1}^{x_N} \qquad (2.19)$$

and

$$\sum_{j=1}^{N} \{\langle \alpha_i\ ,\ \alpha_j\rangle/\delta t + \tfrac{1}{6}\,\delta t\,\langle [d(x)\ \alpha_i]'\ ,\ c(x)\ \alpha_j'\rangle\}\ [\eta_j^{n+1} - \eta_j^n] =$$

$$\sum_{j=1}^{N} \{-\langle \alpha_i\ ,\ d(x)\ \alpha_j'\rangle + \tfrac{1}{2}\,\delta t\,\langle d(x)\ \alpha_i\ ,\ [p(x)\ \alpha_j]'\rangle -$$

$$\tfrac{1}{6}\,(\delta t)^2\,\langle d(x)\ \alpha_i\ ,\ [(p(x))^2\ \alpha_j]'\rangle\}\ v_j^n + \sum_{j=1}^{N} \{-\tfrac{1}{2}\,\delta t\,\langle [d(x)\ \alpha_i]'\ ,$$

$$c(x)\ \alpha_j'\rangle + \tfrac{1}{6}\,(\delta t)^2\,\langle [d(x)\ \alpha_i]'\ ,\ p(x)\ c(x)\ \alpha_j'\rangle\}\ \eta_j^n +$$

$$\tfrac{1}{6}\,\delta t\,[d(x)\ c(x)\ (\eta_x^{n+1} - \eta_x^n)\ \alpha_i]_{x_1}^{x_N} + \tfrac{1}{2}\,\delta t\,[d(x)\ c(x)\ \eta_x^n\ \alpha_i]_{x_1}^{x_N} -$$

$$\tfrac{1}{6}\,(\delta t)^2\,[d(x)\ p(x)\ c(x)\ \eta_x^n\ \alpha_i]_{x_1}^{x_N}, \qquad (2.20)$$

for $i = 1(1)N$, in which $\langle \cdot , \cdot \rangle$ is defined by

$$\langle \xi , \chi \rangle = \int_{x_1}^{x_N} \xi(x)\, \chi(x)\, dx, \tag{2.21}$$

for integrable functions ξ and χ. Note that the last three terms on the right-hand sides of (2.19) and (2.20) are boundary terms, which effect only the boundary nodes at which Dirichlet conditions are not prescribed.

As is standard practice with finite-element methods, the local 4x4 matrices and 4x1 column vectors are evaluated over each element and then assembled into a global system. The element integrals involving the functions c, d, and p are evaluated (a) using eight-point Gaussian quadrature, and (b) only once, since such integrals are independent of time. The global system at each time level, n, is

$$A\, [\underline{y}^{n+1} - \underline{y}^{n}] = \underline{r}^{n}, \tag{2.22}$$

in which A is a time-independent, symmetric, 2x2-block-tridiagonal, 2Nx2N matrix; $\underline{r}^{n}$ is a known 2Nx1 vector; and

$$\underline{y}^{n} = [v_1^n, \eta_1^n; v_2^n, \eta_2^n; \ldots; v_N^n, \eta_N^n]^T. \tag{2.23}$$

We now consider the imposition of boundary conditions. Equations (2.2) are discretised in the standard way; namely, as

$$\left.\begin{aligned} v_N^n &= 0 \\ \eta_1^n &= f(t^n) \end{aligned}\right\}, \quad n = 0(1)M, \tag{2.24}$$

where M is the number of time steps and

$$t^n = n\,\delta t, \quad n = 0(1)M, \tag{2.25}$$

in which

$$\delta t = T/M. \tag{2.26}$$

Still lacking, however, are expressions for v_x^n at $x = x_1$ and η_x^n at $x = x_N$ in the boundary terms of Equations (2.19) and (2.20). In the case of the first condition, we proceed as follows. By evaluating (2.8) at $x = 0$, we may write

$$v_x(0,t) = -\,b(0)\,\eta_t(0,t), \quad 0 \le t \le T, \tag{2.27}$$

using the second of (2.6). Since $\eta(0,t)$ is $f(t)$ for all t in question (see (2.2)), it follows that

$$v_x(0,t) = -\,b(0)\,f'(t), \quad 0 \le t \le T. \tag{2.28}$$

A similar treatment conducted on η produces

$$\eta_x(L,t) = 0, \quad 0 \le t \le T. \tag{2.29}$$

We now incorporate (2.24), (2.28), and (2.29) into (2.22) to obtain the modified global system of

$$\tilde{\underline{A}} \, [\underline{y}^{n+1} - \underline{y}^{n}] = \tilde{\underline{r}}^{n}, \tag{2.30}$$

say, in which $\underline{y}^{n}$ is defined in Equation (2.23). In practice, (2.30) is inverted for $\underline{y}^{n+1} - \underline{y}^{n}$ (using a 2x2-block-tridiagonal-matrix solver) at each time level, n, then $\underline{y}^{n+1}$ is determined.

Finally, we satisfy (2.3) using the iteration algorithm which follows. (i) Set $t = 0$ and choose $\tilde{v}$ and $\tilde{\eta}$ to be 0 and f(0) respectively. (ii) Integrate the problem forward in time (by assembling and solving (2.30)) until the tidal period, T, is reached. (iii) Investigate the satisfaction of

$$\| \tilde{v}(\cdot,T) - \tilde{v}(\cdot,0) \|_{\infty} < \epsilon \max\{ \| \tilde{v}(\cdot,0) \|_{\infty} , 1 \} \tag{2.31}$$

and

$$\| \tilde{\eta}(\cdot,T) - \tilde{\eta}(\cdot,0) \|_{\infty} < \epsilon \max\{ \| \tilde{\eta}(\cdot,0) \|_{\infty} , 1 \} \tag{2.32}$$

for some convergence tolerance, ϵ. (iv) If both (2.31) and (2.32) are obeyed, then $\tilde{v}$ and $\tilde{\eta}$ are acceptable as periodic solutions; otherwise, update $\tilde{v}$ and $\tilde{\eta}$ according to

$$\left.\begin{aligned} \tilde{v}(x,0) &:= \lambda \, \tilde{v}(x,T) + [1-\lambda] \, \tilde{v}(x,0) \\ \tilde{\eta}(x,0) &:= \lambda \, \tilde{\eta}(x,T) + [1-\lambda] \, \tilde{\eta}(x,0) \end{aligned}\right\}, \quad 0 \le x \le L \tag{2.33}$$

(in which λ ($0 < \lambda \leq 1$) is a relaxation parameter), then return to Stage (ii) with t reset to zero.

2.3 Results for Problem 1

As it is our aim to model flows in the Severn estuary, throughout this subsection we choose the length of the estuary, L, and the friction parameter, p_0, (Birkett, 1985) as

$$\left.\begin{aligned} L &= 50\ 000 \\ p_0 &= 0.0025 \end{aligned}\right\}. \tag{2.34}$$

The tide function, f, is given by

$$f(t) = \zeta \sin(2\pi t/T), \quad 0 \leq t \leq T, \tag{2.35}$$

where ζ is the tidal amplitude (which assumes the value of unity unless otherwise stated). The value of the relaxation parameter is

$$\lambda = \tfrac{1}{2}. \tag{2.36}$$

In the case of the ensuing graphical output, we take

$$\epsilon = 10^{-2}, \tag{2.37}$$

corresponding to less than a 1 % relative error; whereas, for accuracy

tests, we take

$$\epsilon = 10^{-5}, \tag{2.38}$$

as it is imperative to have a "converged" solution for such analysis. The cross-sectional-area function is

$$a(x) = b(x)\, h(x), \quad 0 \leq x \leq L, \tag{2.39}$$

where b and h are defined to be

$$\left.\begin{aligned} b(x) &= 15\ 000 \\ h(x) &= 15 \end{aligned}\right\}, \quad 0 \leq x \leq L, \tag{2.40}$$

for the constant-coefficient problem, and

$$\left.\begin{aligned} b(x) &= 40\ 000 - 0.74\, x \\ h(x) &= 25 - 0.0004\, x \end{aligned}\right\}, \quad 0 \leq x \leq L, \tag{2.41}$$

for the linear-coefficient one.

The tidal period (in seconds) of the Severn estuary is given by

$$T = 44\ 714. \tag{2.42}$$

Using this value, together with 21 nodes and 240 time steps (yielding a C.F.L. number of approximately 0.904), and with the constant

coefficients of (2.40), we obtain Figures 2a-e (after 8 iterations). The upper graph of each figure is of the fluid velocity (i.e., flow divided by cross-sectional area) against distance along the estuary; the lower one, elevation against distance. In all figures, the graphs are quite linear. The initial non-negative velocity profile in Figure 2a is greatly decreased at the quarter period (in Figure 2b). At 22 357 seconds, the velocity profile is a reflection in the horizontal axis of the initial profile; also, the three-quarter-period velocity is related to the quarter-period one in the same way. Finally, the initial velocity distribution is reproduced after 44 714 seconds in Figure 2e. The elevation in Figures 2a-e behaves in a manner similar to the velocity: the initial non-positive values of small magnitude become very positive (in Figure 2b), noticeably decrease (in Figure 2c), further decrease (in Figure 2d) to negative values, then increase to the initial profile (in Figure 2e).

On replacing the constant-coefficient data of (2.40) by the linear data of (2.41), we obtain Figures 3a-e. The behaviour of the velocity and elevation is identical to that of the the previous case. The differences between Figures 2a-e and 3a-e are that, in the case of the latter, (a) both the velocity and elevation are smaller in magnitude, and (b) the velocity profiles contain considerably more curvature.

We now perform some tests on the constant-coefficient model. With 65 nodes and 16 time steps, we choose a tidal period of 1030.633 seconds to enforce a C.F.L. number of one. The resulting velocity and elevation graphs (after 62 iterations) are depicted in Figures 4a-e.

All curves, which are well resolved, are damped sines and cosines which exhibit the reflection property of the previous runs. On using the same tidal period, but with 33 nodes and 8 time steps, we obtain Figures 5a-e; Figures 6a-e result when 16 nodes and 4 time steps are used. The resolution (when simulating with a unit C.F.L. number), which is excellent in all cases, is tested to its limit in Figures 6a-e. On reducing the C.F.L. number to $\frac{1}{2}$, by using 65 nodes and 16 time steps with a tidal period of 515.316 seconds, we obtain the extremely wavy graphs of Figures 7a-e. Once again, the resolution of the velocity and elevation is excellent.

We now investigate the accuracy of the Taylor-Galerkin Method on the shallow-water problem with the constant-coefficient data of (2.40) and the tidal period of (2.42). Tables 1 to 4 contain the exact value of the velocity or elevation (obtained via an analytic solution derived using the method employed in Subsection 3.2) at selected points along the estuary at certain times. The columns headed e_1, e_2, and e_3 contain values of 10^5 times the deviations from the exact values when using node/time-step numbers of (11,120), (21,240), and (41,480) respectively. We analyse the velocities in Tables 1 and 2, and the elevations in Tables 3 and 4; the output time is 0 seconds for Tables 1 and 3, and 11 178.5 seconds (i.e., the quarter period) for Tables 2 and 4.

Throughout Tables 1 to 4, the columns headed e_1 contain very accurate values, those in columns e_2 are extremely accurate, and those in e_3 are almost exact to five decimal places. The general trends are that (a) the velocity deviations decrease as the distance increases, and

(b) the elevation ones remain approximately constant (except those at a distance of zero kilometres, at which a Dirichlet condition is imposed). The deviations of Tables 1 to 4 indicate that the Taylor-Galerkin Method is approximately second-order accurate (a result that conflicts with the third order established by Donea (1984)).

The c.p.u. times consumed on a Norsk-Data Nord 500 mini computer for simulations including node/time-step numbers of (11,120), (21,240), and (41,480) are approximately 21, 76, and 295 seconds respectively, when ϵ is 10^{-5}. The corresponding times when ϵ is 10^{-1} are 10, 35, and 133 seconds. When ϵ is decreased from 10^{-1} to 10^{-5}, the number of iterations increases from 8 to 18. These values illustrate that (i) the computer times are increased by a factor of almost four when the element and time-step numbers are simultaneously doubled, and (ii) more than twice as much c.p.u. time and more than double the number of iterations are required when the desired accuracy is reduced from 1 % to 0.001 %.

Finally, consider the variation of the velocity and elevation with the tidal amplitude, ζ (of (2.35)). Numerical evidence suggests that both the velocity and elevation are proportional to the tidal amplitude (to within an amount ϵ); hence, the theoretical result is sufficiently adhered to.

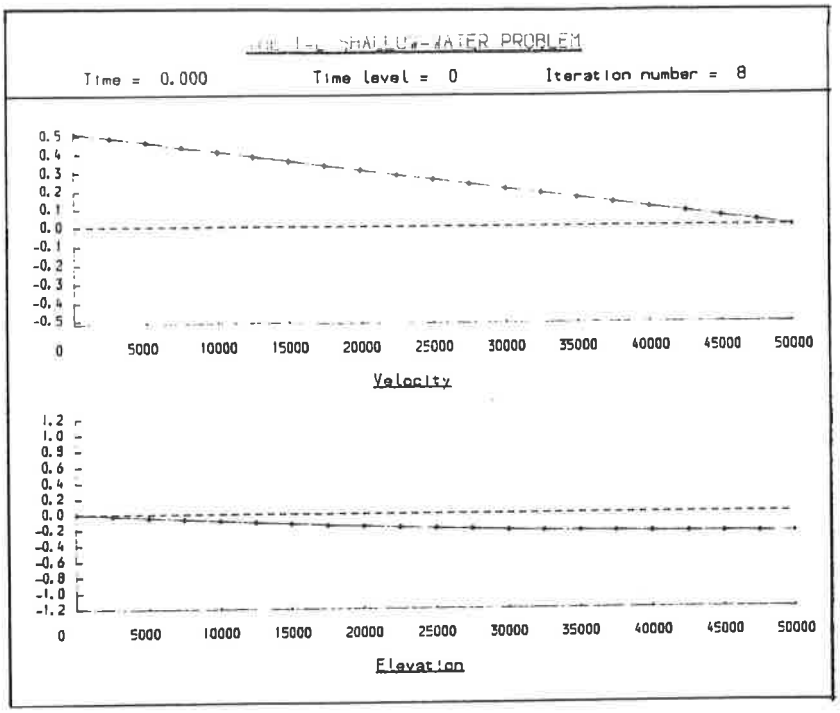

Figure 2a

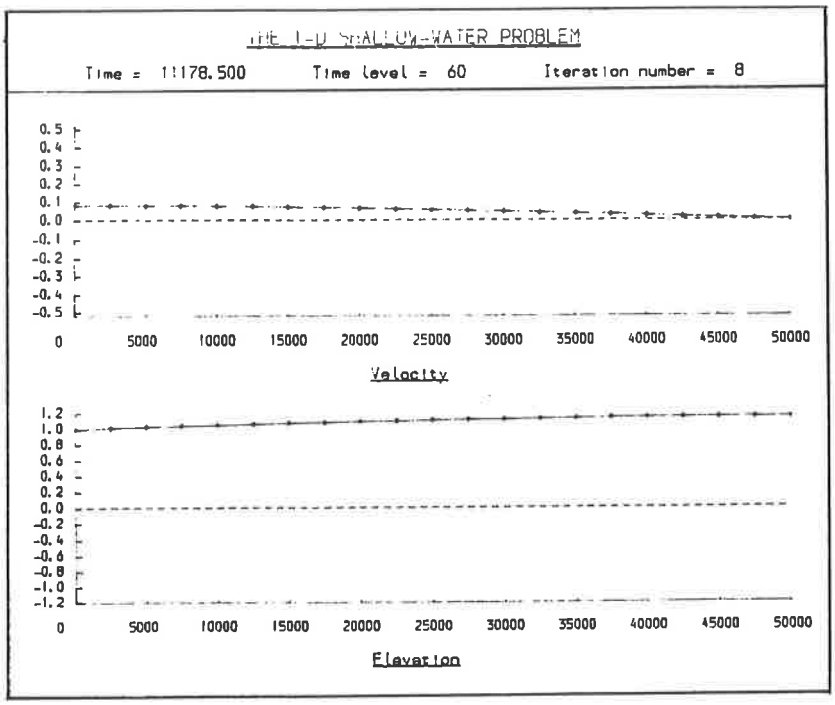

Figure 2b

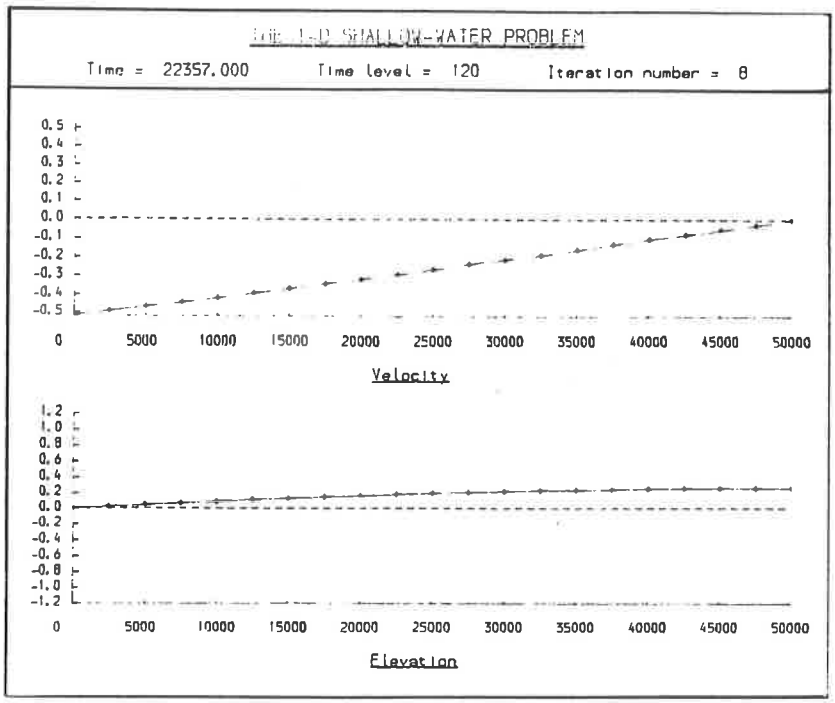

Figure 2c

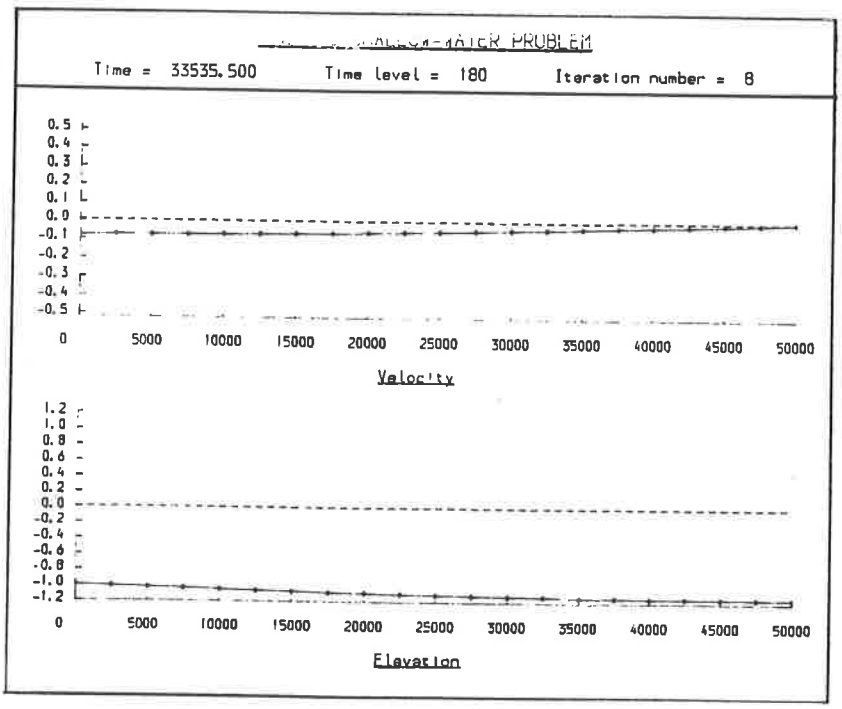

Figure 2d

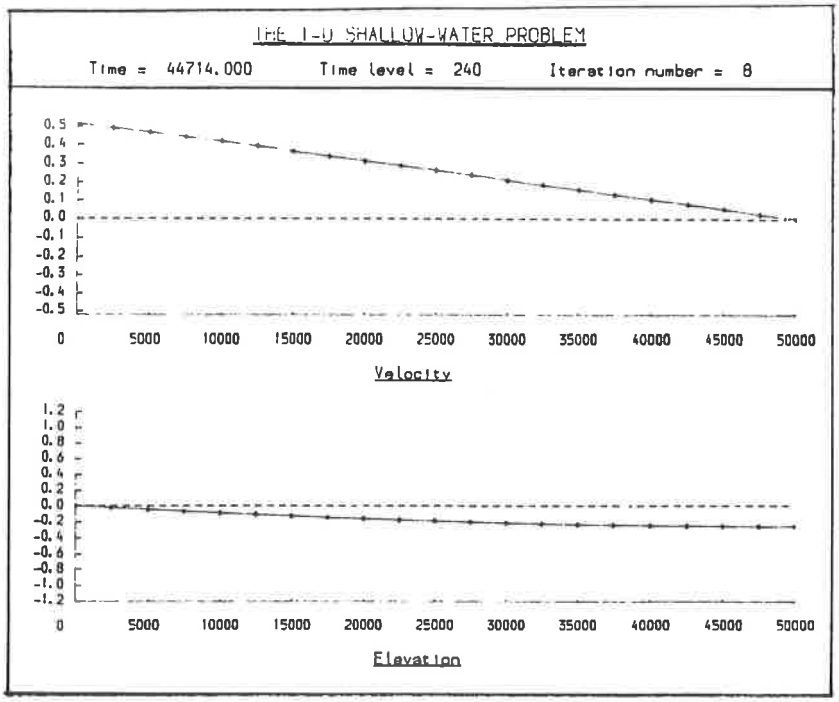

Figure 2e

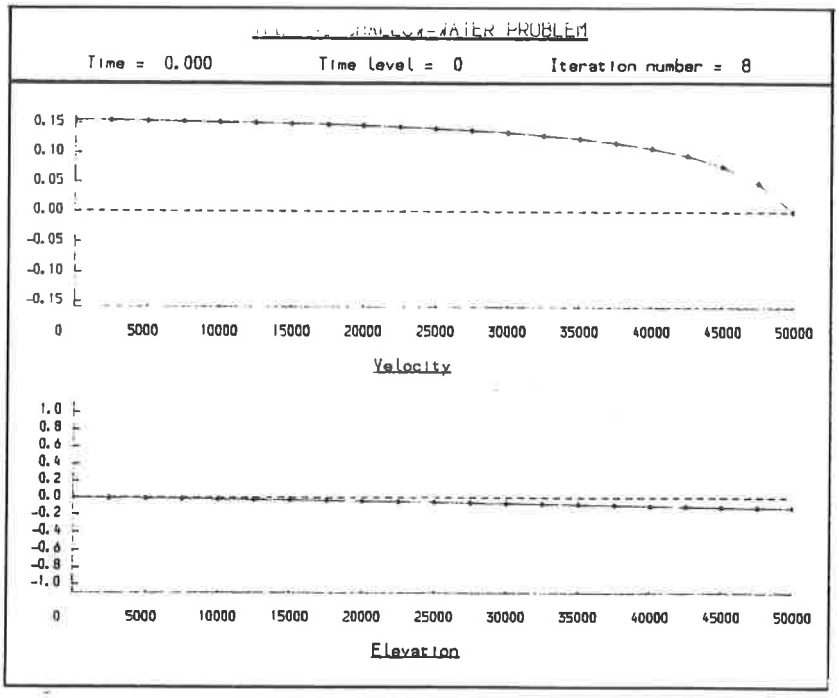

Figure 3a

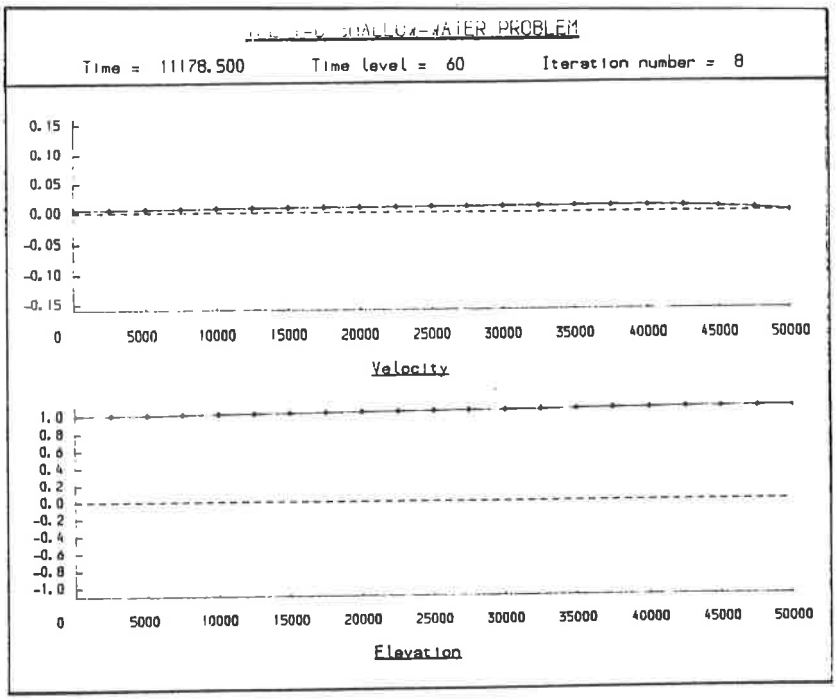

Figure 3b

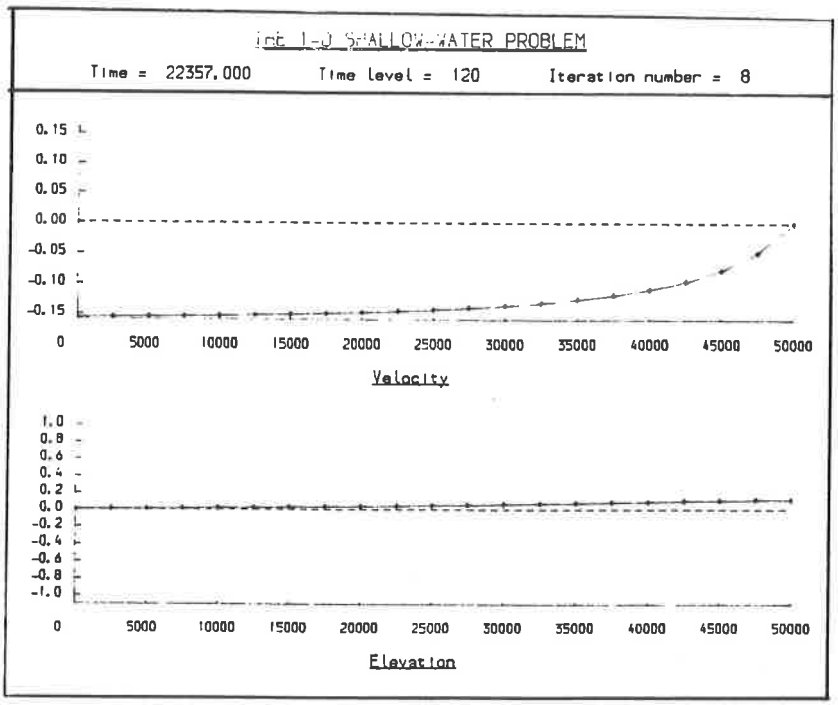

Figure 3c

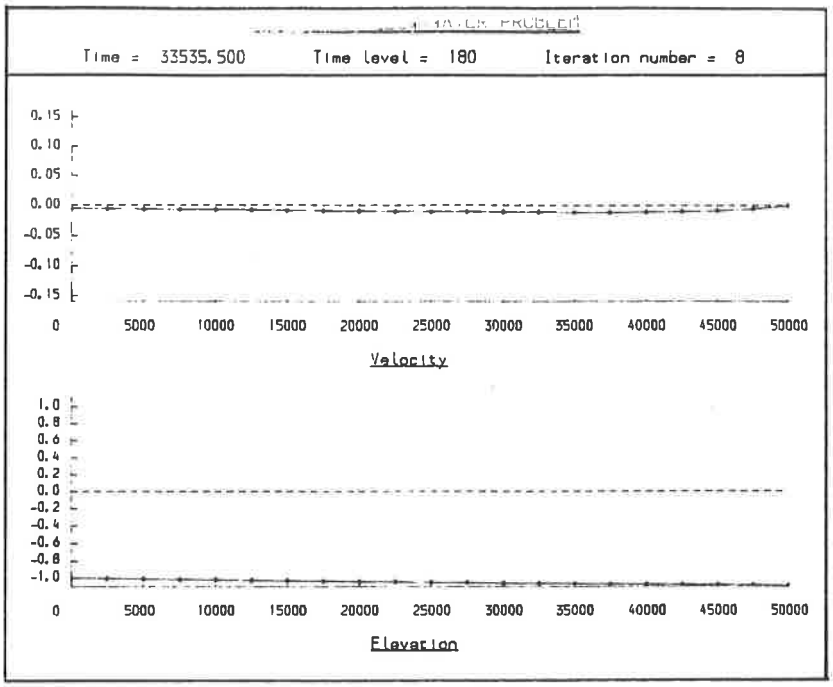

Figure 3d

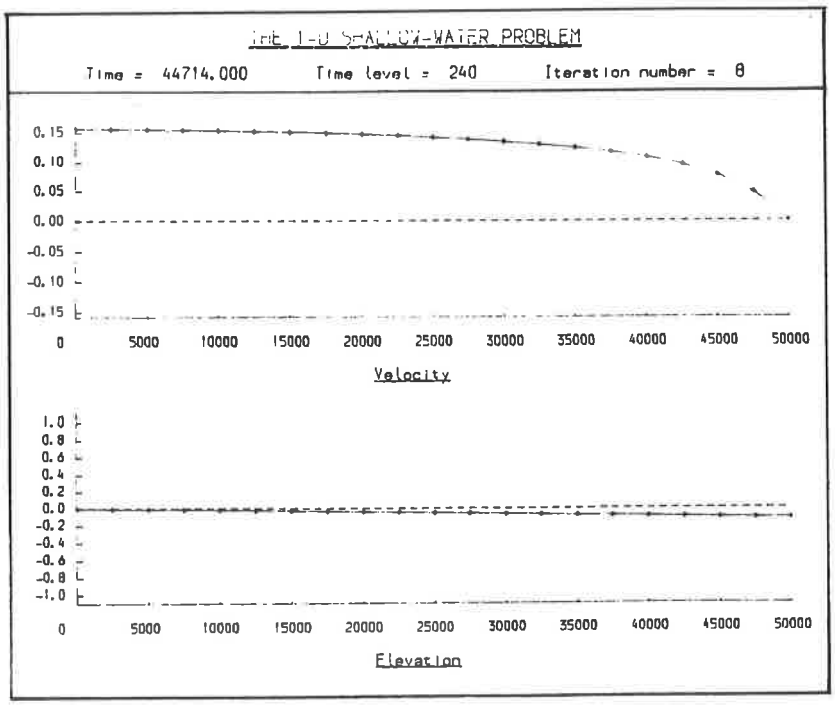

Figure 3e

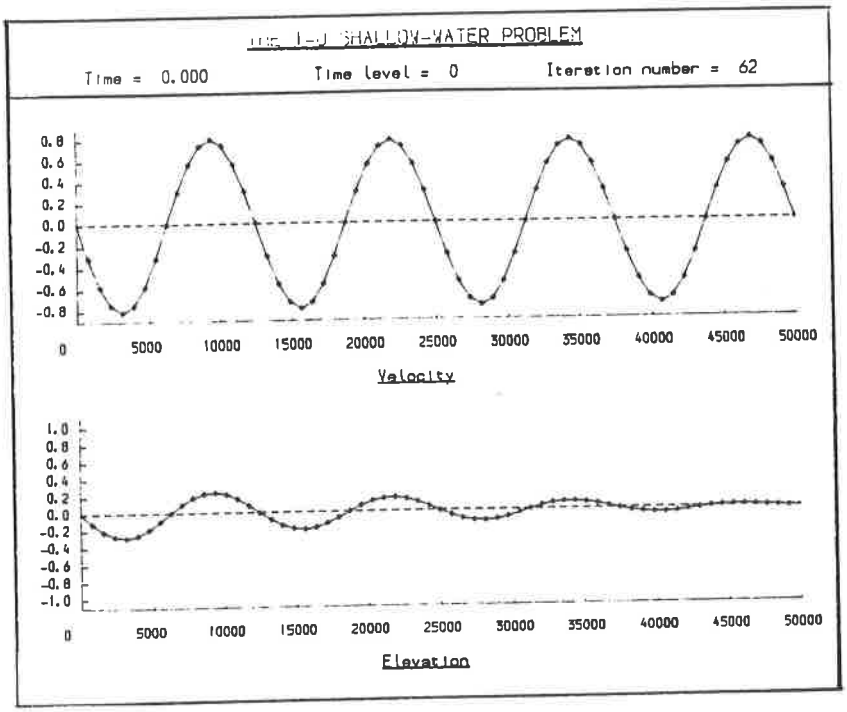

Figure 4a

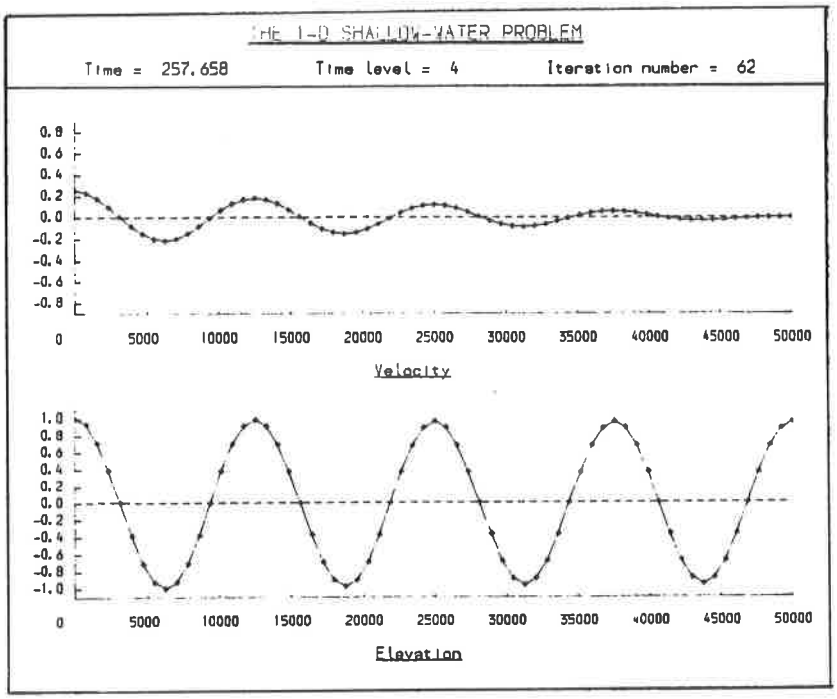

Figure 4b

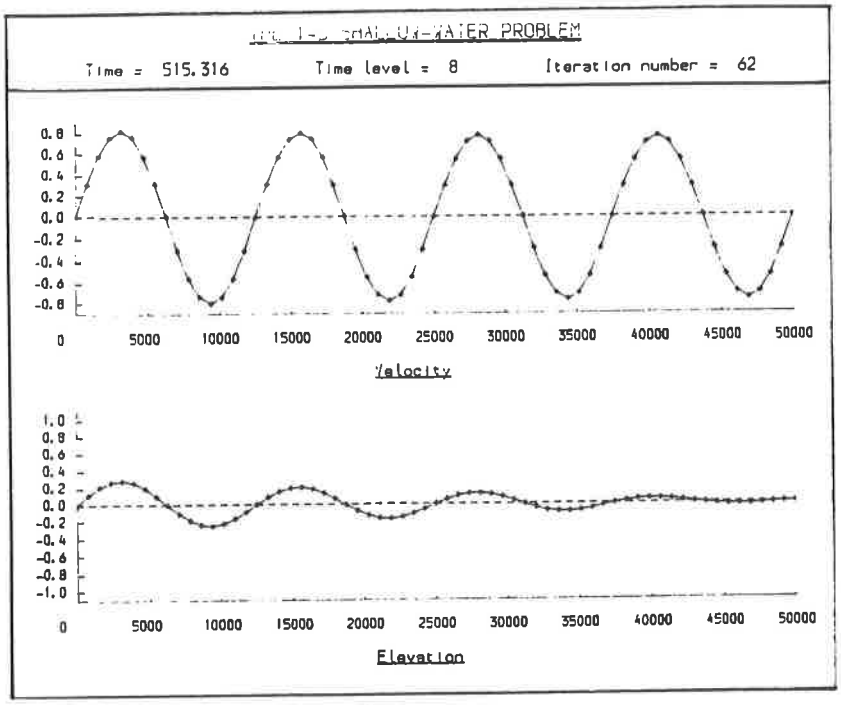

Figure 4c

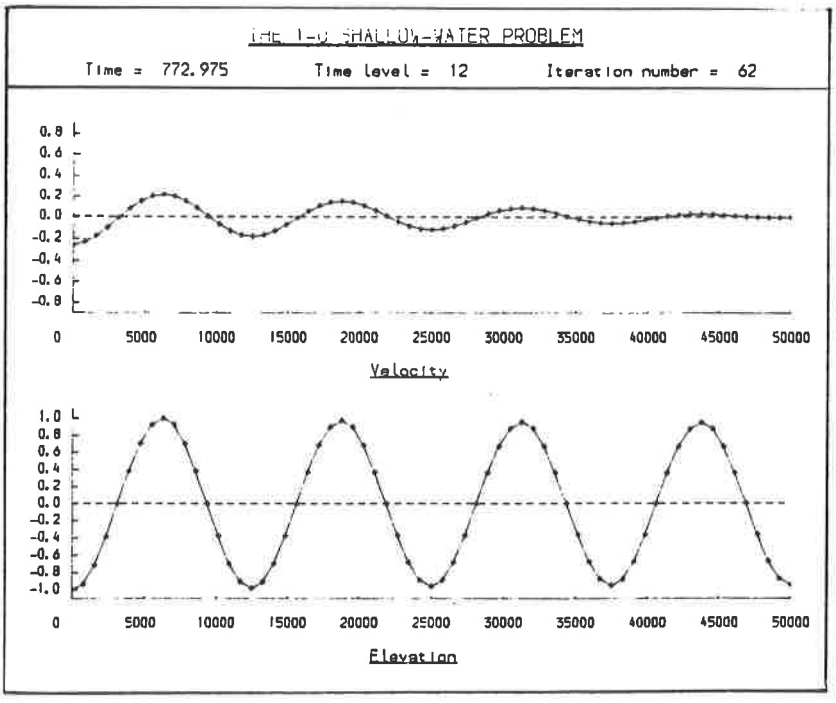

Figure 4d

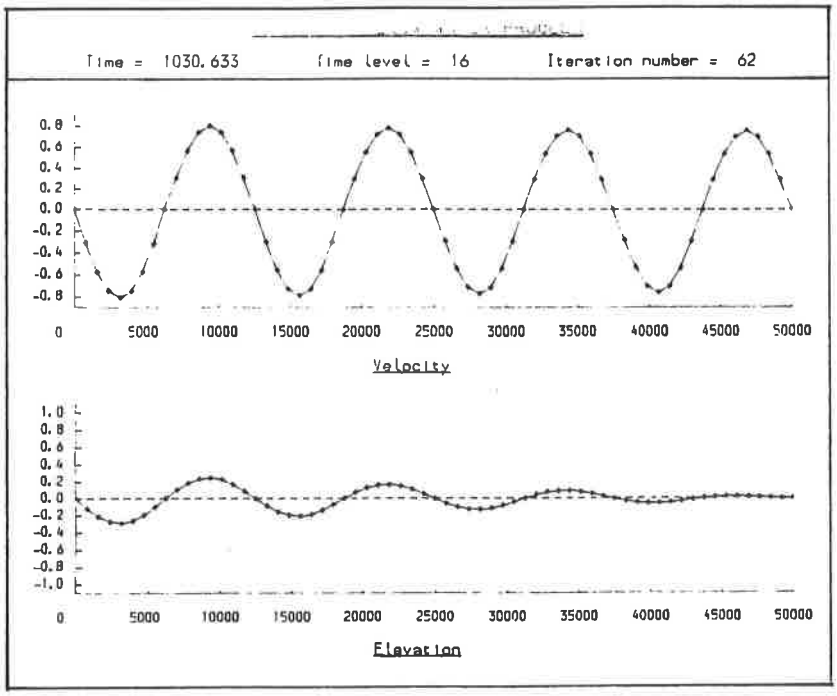

Figure 4e

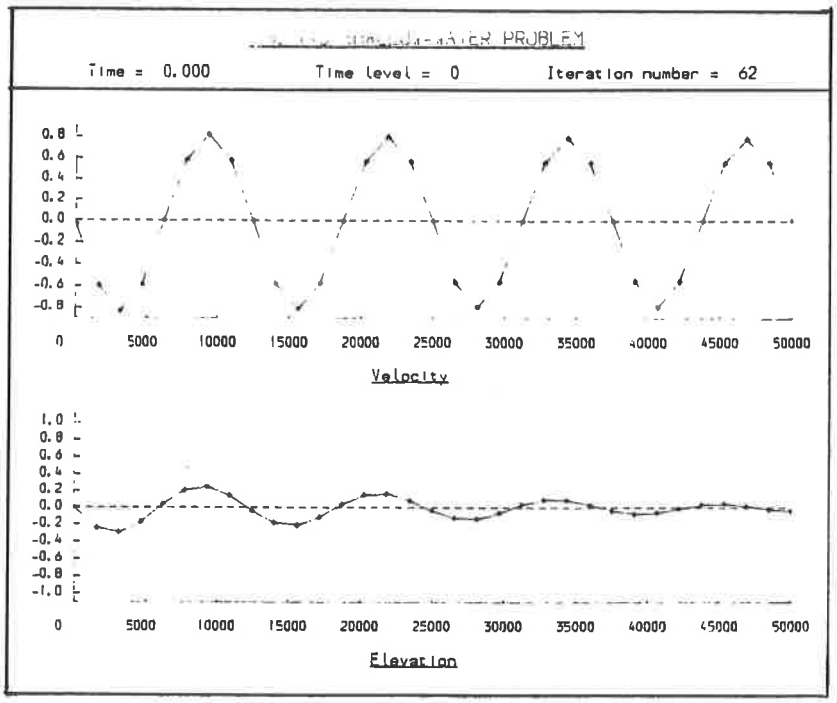

Figure 5a

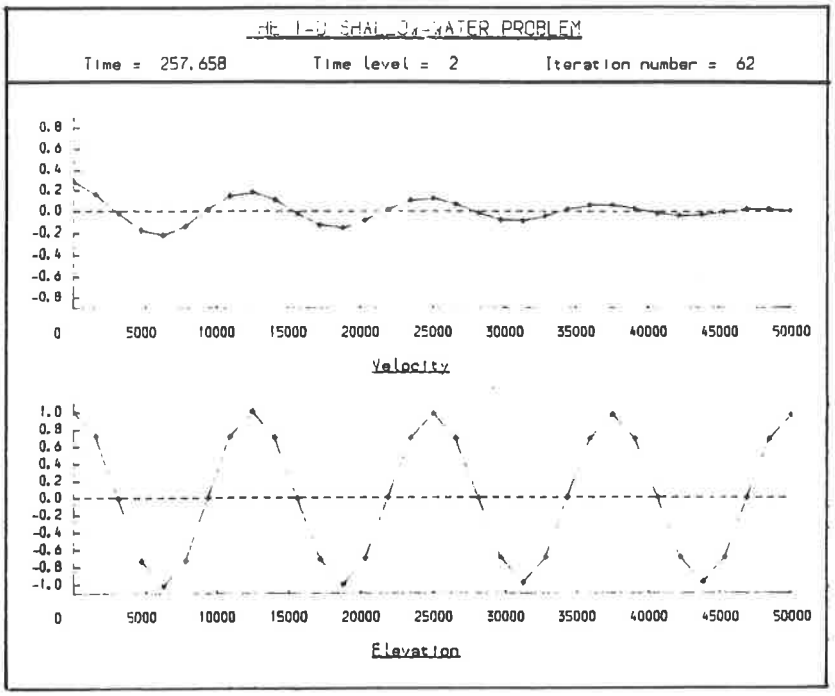

Figure 5b

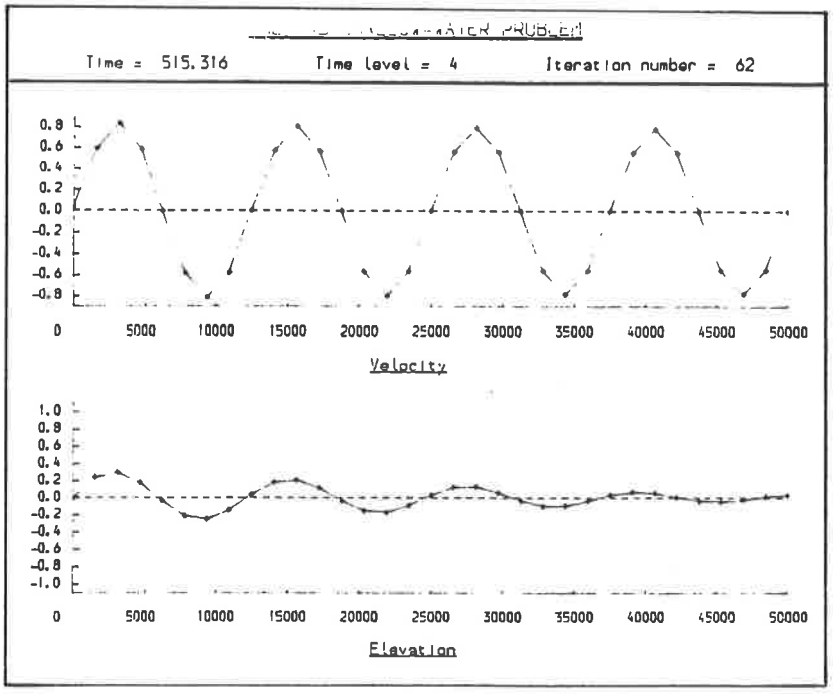

Figure 5c

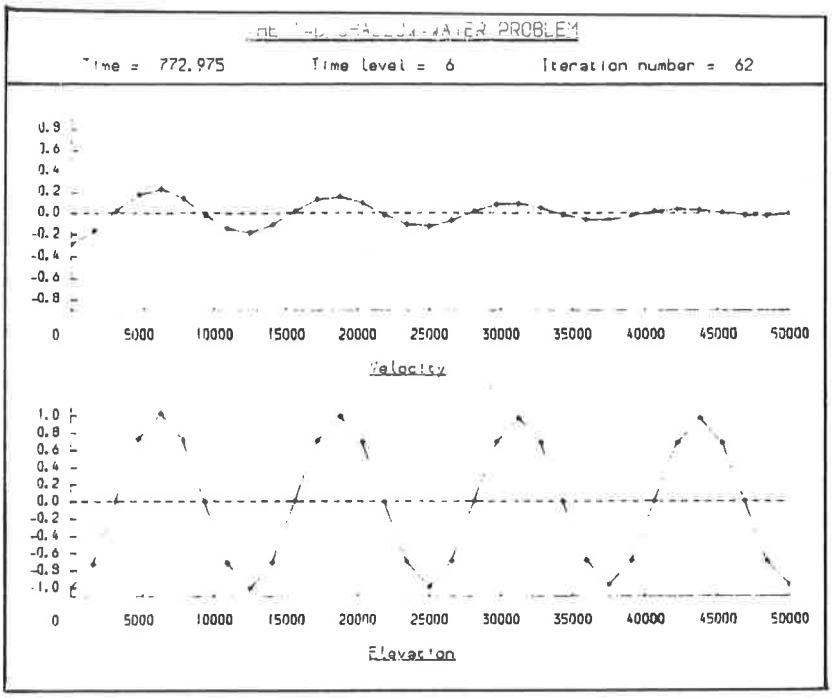

Figure 5d

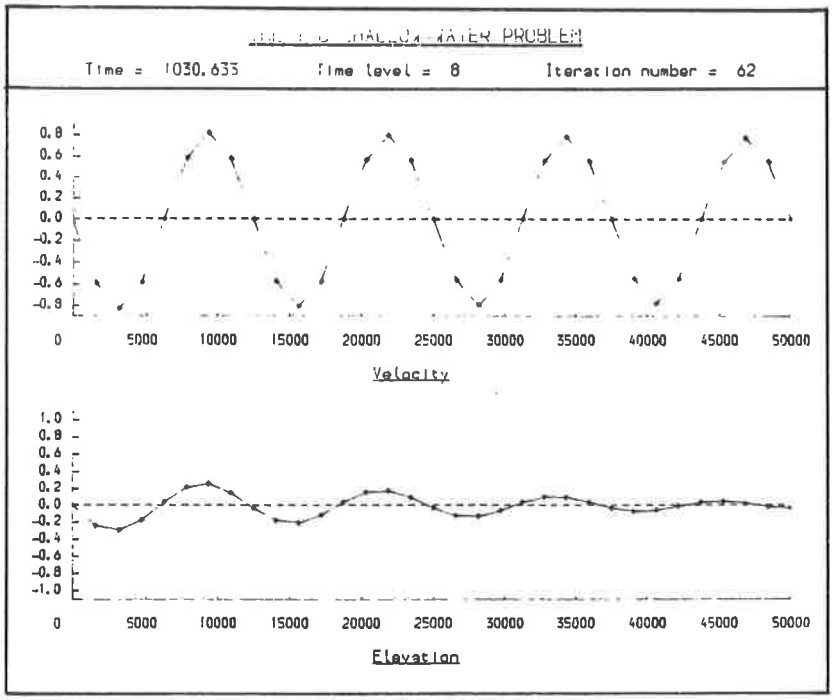

Figure 5e

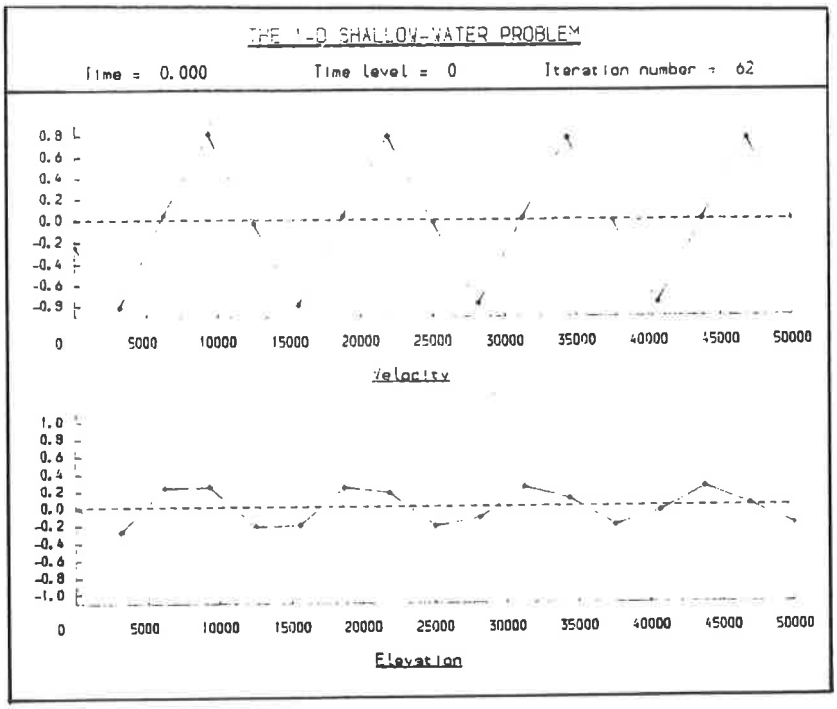

Figure 6a

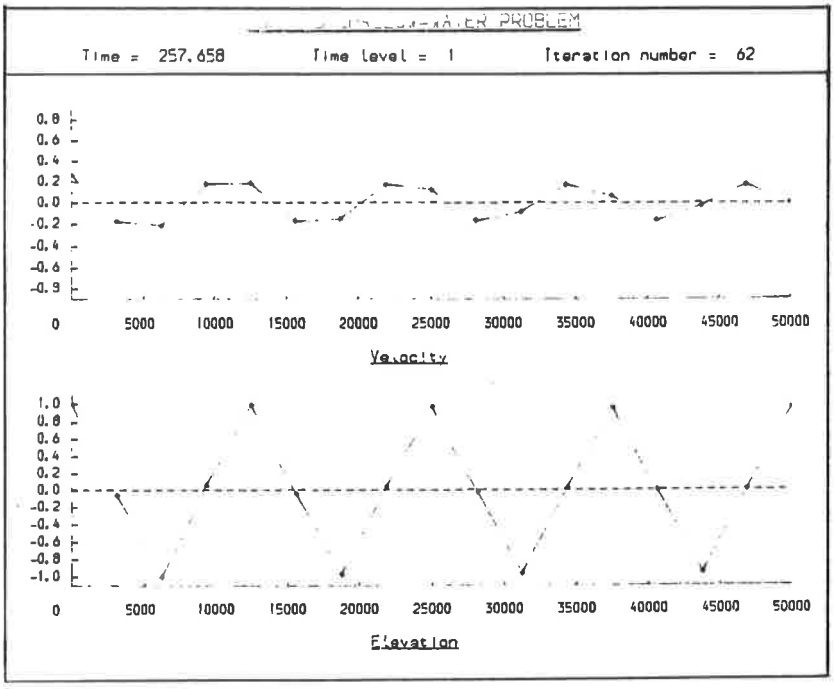

Figure 6b

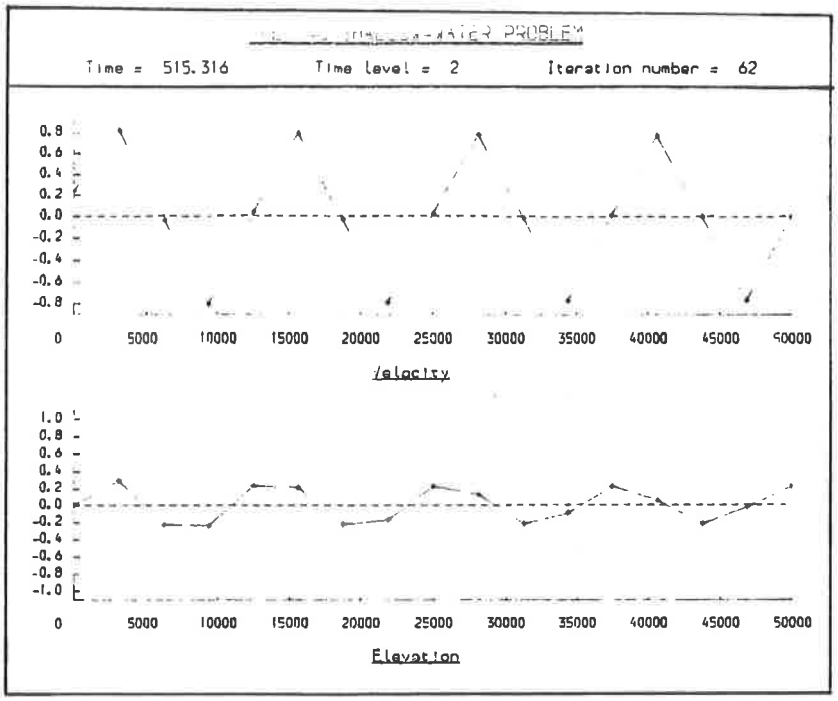

Figure 6c

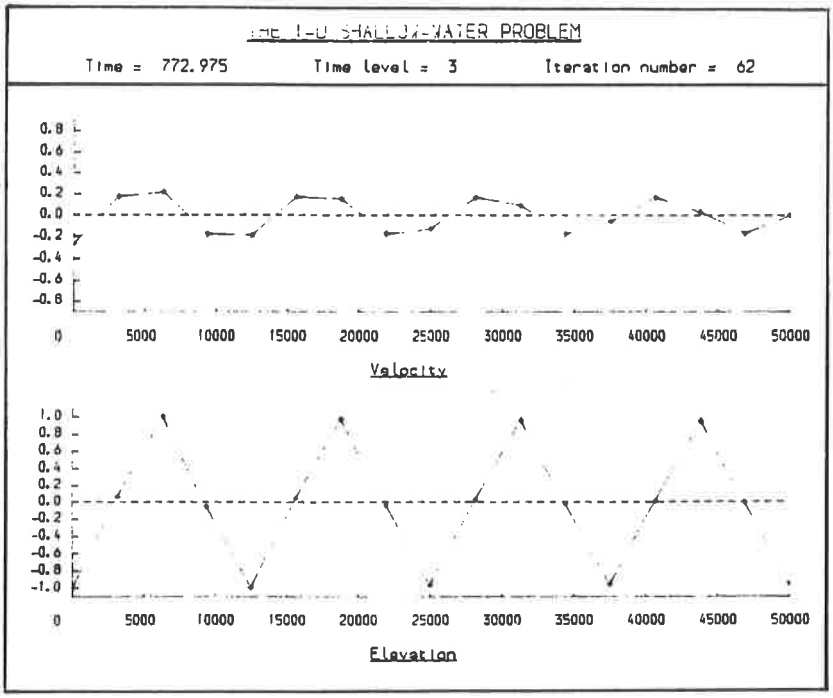

Figure 6d

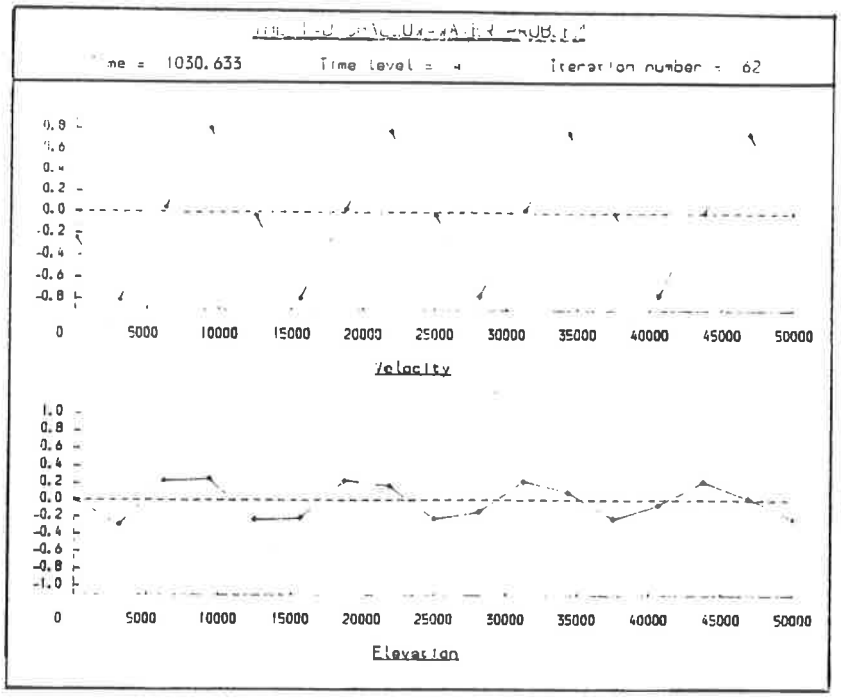

Figure 6e

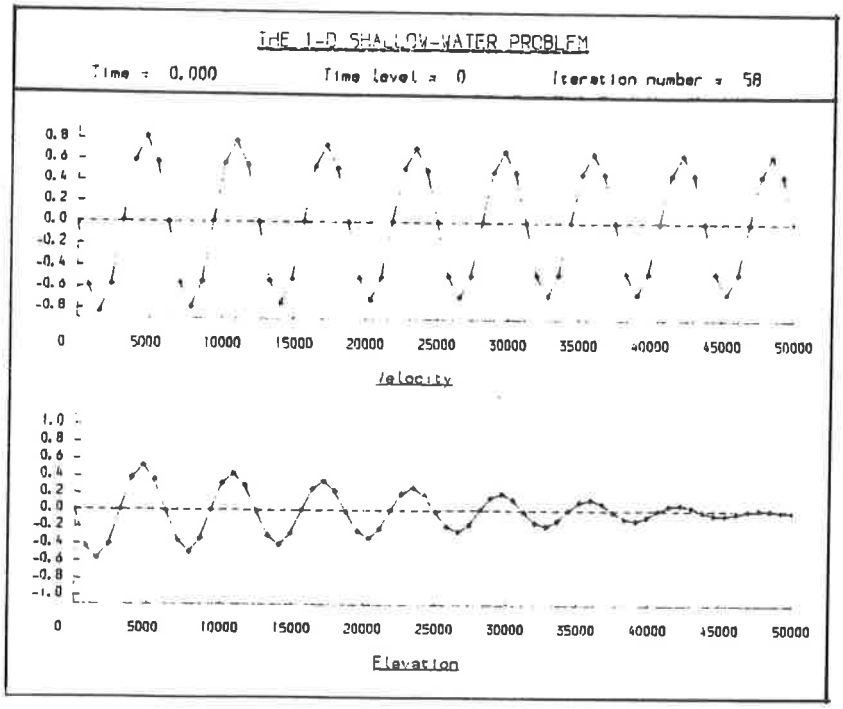

Figure 7a

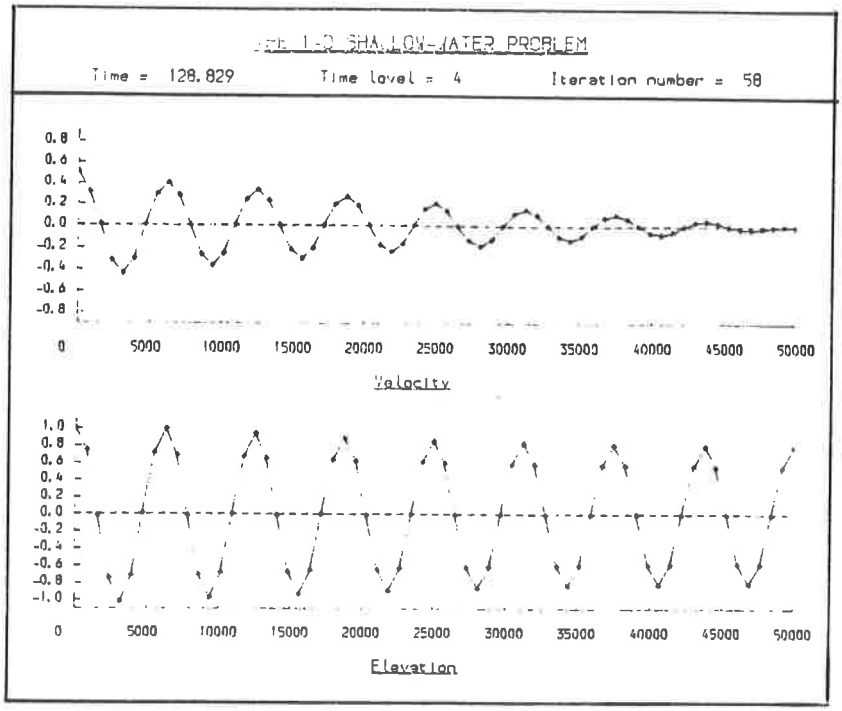

Figure 7b

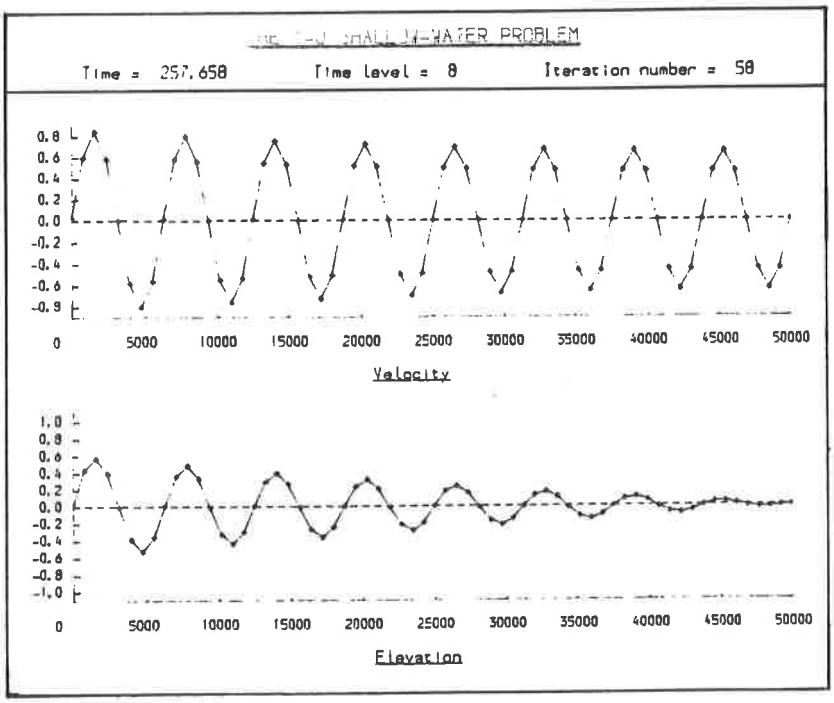

Figure 7c

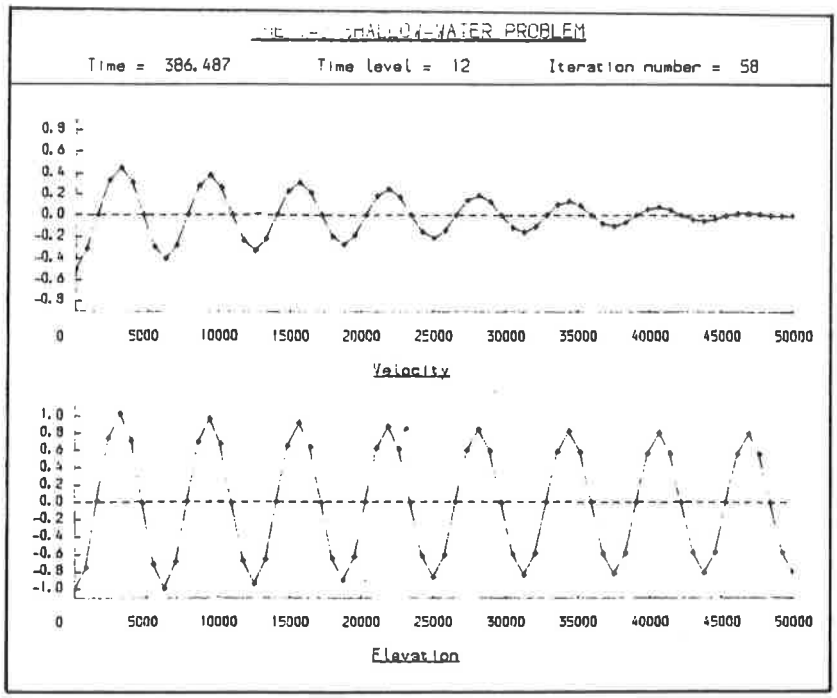

Figure 7d

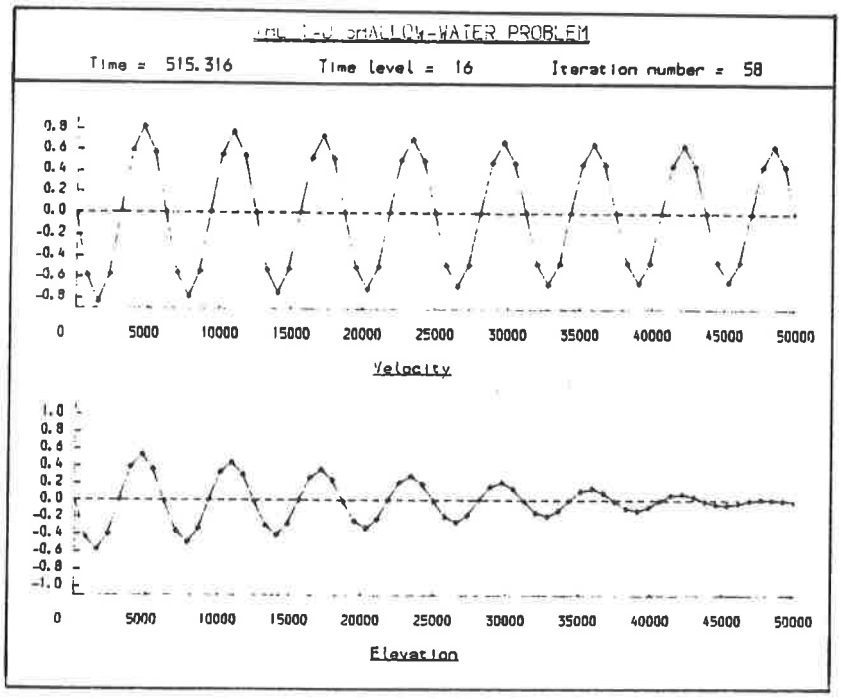

Figure 7e

Distance (km)	Exact Velocity	e_1	e_2	e_3
0	0.51412	17	4	1
5	0.46660	-11	-2	0
10	0.41783	-8	-2	-1
15	0.36796	-7	-2	-1
20	0.31714	-6	-1	0
25	0.26551	-5	-1	0
30	0.21320	-4	-1	-1
35	0.16036	-3	-1	-1
40	0.10713	-2	0	0
45	0.05363	-1	0	0
50	0.00000	0	0	0

Table 1

Distance (km)	Exact Velocity	e_1	e_2	e_3
0	0.08021	-35	-9	-2
5	0.07908	-14	-4	-1
10	0.07583	-16	-4	-1
15	0.07067	-13	-3	-1
20	0.06380	-12	-3	-1
25	0.05546	-10	-3	-1
30	0.04588	-8	-2	0
35	0.03529	-6	-2	-1
40	0.02395	-4	-1	0
45	0.01210	-2	-1	0
50	0.00000	0	0	0

Table 2

Distance (km)	Exact Elevation	e_1	e_2	e_3
0	0.00000	0	0	0
5	-0.04740	37	9	2
10	-0.09054	38	10	3
15	-0.12920	39	10	2
20	-0.16314	40	10	2
25	-0.19218	42	10	3
30	-0.21616	43	11	3
35	-0.23495	43	11	3
40	-0.24844	44	11	3
45	-0.25657	44	11	3
50	-0.25928	45	11	3

Table 3

Distance (km)	Exact Elevation	e_1	e_2	e_3
0	1.00000	0	0	0
5	1.02836	-28	-6	-1
10	1.05345	-24	-6	-2
15	1.07537	-23	-6	-1
20	1.09419	-23	-6	-2
25	1.10999	-22	-6	-1
30	1.12283	-22	-6	-1
35	1.13276	-21	-5	-1
40	1.13982	-21	-6	-1
45	1.14405	-21	-5	-1
50	1.14545	-21	-6	-2

Table 4

3. THE SHALLOW-WATER PROBLEM WITH A BARRIER

In this section we introduce a barrier into Problem 1 to produce Problem 2, which is formulated in Subsection 3.1. Subsection 3.2 contains the derivation of an analytic solution of Problem 2 with simple data. We describe the numerical techniques used to solve the new problem in Subsection 3.3, then display and discuss some results in 3.4.

3.1 Mathematical Formulation of Problem 2

As is the case in Subsection 2.1, the fluid velocity, v, and elevation, η, are governed by the partial differential equations in (2.1) and satisfy the boundary and initial conditions of (2.2) and (2.3). Suppose now that a barrier is inserted at ℓ metres along the estuary, where $0 < \ell < L$. We require that the fluid flow be continuous across the barrier and proportional to the head difference at the barrier, and so impose the simple linear conditions

$$\left.\begin{aligned} v(\ell^-,t) &= \kappa\,[\eta(\ell^-,t) - \eta(\ell^+,t)] \\ v(\ell^+,t) &= \kappa\,[\eta(\ell^-,t) - \eta(\ell^+,t)] \end{aligned}\right\}, \quad 0 \le t \le T, \tag{3.1}$$

where κ is the barrier constant, and ℓ^- and ℓ^+ denote points to the immediate left and right of the barrier respectively. Therefore, the mathematical formulation of Problem 2 consists of (2.1)-(2.3) and (3.1).

The energy, E, (in Watt seconds) derived from the tidal-power scheme is given by

$$E = \rho\, g\, \kappa \int_0^T [\eta(\ell^-, t) - \eta(\ell^+, t)]^2 \, dt, \tag{3.2}$$

where ρ is the density of the water. In practice, we evaluate (3.2) (on each iteration) using the Trapezium Rule.

3.2 An Analytic Solution of Problem 2

Suppose that the functions a, b, and h assume the constant values of $\bar{a}$, $\bar{b}$, and $\bar{h}$, then we have

$$\left.\begin{aligned} a(x) &= \bar{a} \\ b(x) &= \bar{b} \\ p(x) &= p_0/\bar{h} \end{aligned}\right\}, \quad 0 \le x \le L. \tag{3.3}$$

Now the tide function f (of the second condition in Equation (2.2)) is typically given by (2.35); in fact, in this subsection we shall consider

$$f(t) = e^{\iota\omega t}, \tag{3.4}$$

in which ι is the square root of -1 and

$$\omega = 2\pi/T. \tag{3.5}$$

Let us suppose that

$$\left.\begin{aligned} v(x,t) &= e^{\iota\omega t}\, w(x) \\ \eta(x,t) &= e^{\iota\omega t}\, z(x) \end{aligned}\right\}, \quad 0 \le x \le L,\ 0 \le t \le T, \tag{3.6}$$

in which w and z are functions to be determined. Note that (a) both v and η satisfy the periodic property, (2.3), and (b) we may recover the sine form of f (from (3.4)) by taking the imaginary parts in (3.6), once w and z are found.

On substituting (3.3) and (3.6) into (2.1) we arrive at

$$\left.\begin{aligned} [\iota\,\omega + p_0/\bar{h}]\, w(x) + g\,\bar{a}\, z'(x) &= 0 \\ \iota\,\omega\,\bar{b}\, z(x) + w'(x) &= 0 \end{aligned}\right\}, \quad 0 \le x \le L. \tag{3.7}$$

Elimination of w from (3.7) produces

$$z''(x) + \gamma^2 z(x) = 0, \quad 0 \le x \le L, \tag{3.8}$$

in which

$$\gamma^2 = \frac{\bar{b}\,\omega^2}{g\,\bar{a}} - \iota\,\frac{\bar{b}\,p_0\,\omega}{g\,\bar{a}\,\bar{h}}. \tag{3.9}$$

The boundary conditions, corresponding to (2.2), for z are

$$z(0) = 1 \tag{3.10}$$

and, using the first equation of (3.7),

$$z'(L) = 0. \tag{3.11}$$

The barrier conditions, (3.1), become

$$\left.\begin{aligned} z'(\ell^-) &= \beta\,[z(\ell^-) - z(\ell^+)] \\ z'(\ell^+) &= \beta\,[z(\ell^-) - z(\ell^+)] \end{aligned}\right\}, \tag{3.12}$$

where

$$\beta = -\frac{\kappa\, p_0}{g\,\bar{a}\,\bar{h}} - \iota\,\frac{\kappa\,\omega}{g\,\bar{a}}. \tag{3.13}$$

In order to solve the simplified problem we must therefore (i) solve (3.8) subject to (3.10)-(3.12) for z, (ii) extract w using the first of (3.7), and (iii) recover v and η via (3.6).

Firstly, we utilise (3.8) to deduce that the general solution for z is

$$z(x) = \left\{\begin{array}{ll} A\,\sin(\gamma x) + B\,\cos(\gamma x), & 0 \le x < \ell \\ C\,\sin(\gamma x) + D\,\cos(\gamma x), & \ell < x \le L \end{array}\right\}, \tag{3.14}$$

where A, B, C, and D are arbitrary constants. Substitution of (3.10)-(3.12) into (3.14) results (after a little algebraic manipulation) in

$$\left.\begin{aligned} B &= 1 \\ D &= \frac{\kappa}{\kappa + \gamma \cos(\gamma\ell)\,[\tan(\gamma L)\cos(\gamma\ell) - \sin(\gamma\ell)]} \end{aligned}\right\}, \qquad (3.15)$$

from which A and C may be assigned by

$$\left.\begin{aligned} A &= [1-D]\tan(\gamma\ell) + D\tan(\gamma L) \\ C &= D\tan(\gamma\ell) \end{aligned}\right\}. \qquad (3.16)$$

So, having determined A, B, C, and D, we are now able to obtain w and z (from (3.14) then the first of (3.7)), and hence v and η (from (3.6)).

In order to obtain an analytic solution for the simplified problem without a barrier, we proceed as follows. Equations (3.3)-(3.6) result in (3.8) and the boundary conditions (3.10) and (3.11). The general solution for z is now the first of (3.14), but is valid for $0 \leq x \leq L$. The values of A and B are now given from (3.10) and (3.11) by

$$\left.\begin{aligned} A &= \tan(\gamma\ell) \\ B &= 1 \end{aligned}\right\}, \qquad (3.17)$$

from which v and η can ultimately be determined using (3.6).

3.3 Numerical Techniques Applied to Problem 2

The Taylor-Galerkin Method of Donea (1984), which is described in

detail in Subsection 2.1, is also applied to Problem 2 ((2.1)-(2.3) and (3.1)). The boundary conditions, (2.2), are again imposed via (2.24), and (2.28) and (2.29) are also included.

Consider now the interface conditions, (3.1), which ensure the continuity of v, but not that of η. To resolve this source of discontinuity, we locate two nodes (x_B and x_{B+1}, say) at the barrier. These coincident nodes facilitate the evaluation of v and η on both the upstream and downstream sides of the barrier (even though these two values for v are the same).

Equations (3.1) are discretised to form two conditions for v; i.e.,

$$\left.\begin{aligned} v_B^n &= \kappa\,[\eta_B^n - \eta_{B+1}^n] \\ v_{B+1}^n &= \kappa\,[\eta_B^n - \eta_{B+1}^n] \end{aligned}\right\}, \quad 0 \le n \le M. \tag{3.18}$$

As it is so with boundary conditions, expressions for η_x are required at nodes at which conditions for v are present. On this occasion, however, it is not possible to obtain explicit conditions for η_x by differentiating the governing conditions ((3.1), in this case). We therefore choose to proceed by approximating $\eta_x(\ell^-,t)$ abd $\eta_x(\ell^+,t)$ for $0 \le t \le T$ using

$$\eta_{x,B}^n = [\eta_B^n - \eta_{B-1}^n]/\Delta_B^-, \quad 0 \le n \le M, \tag{3.19}$$

and

$$\eta^n_{x,B+1} = [\eta^n_{B+2} - \eta^n_{B+1}]/\Delta^+_B, \quad 0 \le n \le M, \tag{3.20}$$

respectively, in which

$$\left.\begin{aligned} \Delta^-_B &= x_B - x_{B-1} \\ \Delta^+_B &= x_{B+2} - x_{B+1} \end{aligned}\right\}. \tag{3.21}$$

We incorporate (3.19) and (3.20) in the *boundary* terms of the Taylor-Galerkin equations for η at the interface; i.e., in the last three terms of (2.20) for $i = B$ and for $i = B+1$. These three terms on the underside of the barrier are then

$$\begin{aligned} &\tfrac{1}{6}\,\delta t\; d(\ell^-)\; c(\ell^-)\; [\eta^{n+1}_B - \eta^{n+1}_{B-1} - \eta^n_B + \eta^n_{B-1}]/\Delta^-_B + \\ &\tfrac{1}{2}\,\delta t\; d(\ell^-)\; c(\ell^-)\; [\eta^n_B - \eta^n_{B-1}]/\Delta^-_B - \\ &\tfrac{1}{6}\,(\delta t)^2\; d(\ell^-)\; p(\ell^-)\; c(\ell^-)\; [\eta^n_B - \eta^n_{B-1}]/\Delta^-_B. \end{aligned}$$

The first of the above is amalgamated with the coefficient matrix (i.e., $\tilde{\underline{A}}$ of (2.30)), and the other two remain on the right-hand side (i.e., in $\tilde{\underline{r}}^n$ of (2.30)). An identical treatment is performed on the equation representing the elevation on the upstream side of the barrier.

Although (3.19) and (3.20) are not highly accurate approximations, they do preserve the block-tridigonal structure of the coefficient matrix; more accurate approximations (for example, those arising from differences over three nodes) would not.

Again, the periodic conditions, (2.3), are imposed by employing an

iteration algorithm: the one described in Subsection 2.2.

3.4 Results for Problem 2

Problem 2, which consists of (2.1)-(2.3) and (3.1), is solved using the Taylor-Galerkin Method of Subsection 2.2, together with the additional treatment of Subsection 3.3. The length of the estuary, L, friction parameter, p_0, tide function, f, and relaxation parameter, λ, are given by (2.34)-(2.36). As before, ϵ is defined by (2.37) in the case of graphical output, and by (2.38) in that of accuracy tests. The barrier is located at

$$\ell = 25\ 000 \tag{3.22}$$

in all simulations.

Suppose that the tidal amplitude (ζ of (2.35)) is unity, the tidal period is given by (2.42), the number of nodes is 22 (of which two are coincident at the barrier), the number of time steps is 240, and the barrier constant is

$$\kappa = 112\ 490 \tag{3.23}$$

(Birkett, 1985,1989). Then we obtain the graphical results of Figures 8a-e on using the constant coefficients of (2.40), and the graphs of Figures 9a-e with the linear coefficients of (2.41).

On comparing the velocity graphs of Figures 8a-e with those of 2a-e (in which the barrier is not present), we observe that the profiles are essentially the same apart from a slight discontinuity in gradient at the barrier. The corresponding elevation graphs are similar on the left-hand side of the 25-kilometre mark, but not on the right-hand side: the presence of the barrier causes a jump in elevation (in Figures 8a-e) at a distance of 25 000 metres along the estuary. These differences are also apparent when comparing the linear-coefficient results of Figures 3a-e with those of 9a-e (which incorporate a barrier).

When the barrier constant is reduced by a factor of two from (3.23) to

$$\kappa = 56\ 245, \tag{3.24}$$

the results in Figures 10a-e and 11a-e are obtained with (2.40) and (2.41) respectively. On comparing Figures 8a-e with 10a-e, and Figures 9a-e with 11a-e, we see that the lower value of κ has the effect of increasing the discontinuities both in v_x and η at the barrier. A further reduction in κ to

$$\kappa = 28\ 212.5, \tag{3.25}$$

leads to the velocity and elevation graphs in Figures 12a-e and 13a-e with (2.40) and (2.41) respectively. In this case, the effect of the lower value of κ is not as dramatic.

We now experiment with the following data: a tidal period of 1030.633 seconds, 66 nodes, 16 time steps, a barrier constant given by (3.23), and the constant coefficients of (2.40). The resulting graphs are depicted in Figures 14a-e, which are quite similar in form to the corresponding 4a-e ones (in which no barrier is present). As expected, though, at the barrier there is a slight discontinuity in v_x, together with a small jump in η. Figures 15a-e are produced when the above data is adjusted to include 32 time steps (causing the C.F.L. number to be halved to $\frac{1}{2}$) and the linear-coefficient data, (2.41). The difference between 14a-e and 15a-e is quite remarkable: in the case of the latter, the velocity and elevation are significantly larger in magnitude (at times, increasing at the right-hand end of the estuary), and the jumps in η are more noticeable.

We now see how the elevation on both sides of the barrier varies with time. The graphs of Figure 16 result when the data which produces Figures 8a-e is utilised. We see that a sine-like curve is present at both the downstream and upstream sides of the barrier (i.e., at $x = 25^-$ and $x = 25^+$). In fact, similar behaviour is observed at these points along the estuary when the data corresponding to all previous elevation graphs is used.

We now investigate the accuracy of the Taylor-Galerkin Method on Problem 2 by using the data which produces Figures 8a-e (but with ϵ given by (2.38), not (2.37)). Exact values of the velocity and elevation are given at points along the estuary at a time of zero seconds in Table 5, in which the columns headed e_V and e_E contain deviations ($x10^5$)

in velocity and elevation respectively. The corresponding values in Table 6 are sampled at the quarter-period; i.e., at 11 178.5 seconds. On comparing the results in Tables 5 and 6 with the corresponding ones in Tables 1 to 4 (that is, those in the column headed e_2), we see that the latest ones are considerably less accurate. The general trend for the elevation deviations is to steadily increase in magnitude until arriving at the downstream side of the barrier (i.e., at 25^-), attain a greatest deviation at 25^+ (possibly due to the inaccurate approximations of (3.19) and (3.20)), then remain approximately constant. The deviations in velocity do not exhibit such a trend, but, like those in elevation, are generally greater in Table 5 than in Table 6. Even though the deviations in Tables 5 and 6 enter the hundreds, the results are in error only in the third decimal place by at most two units, and are accurate to within $\frac{1}{3}$ %.

Table 7 contains values of the energy (in Gigawatt hours) derived from the the tidal-power scheme when the data corresponding to certain graphical results is used. The energies in Table 7 are calculated using $\epsilon = 10^{-1}$; when ϵ is reduced to 10^{-5}, the resulting energies differ from the corresponding tabulated ones by no more than 0.005. The standard problem with the constant data of (2.40) is represented by 8a-e, 10a-e, and 12a-e; the respective values of κ are given by (3.23), (3.24), and (3.25). We see that the energy increases by almost 20 % on reducing κ on the first occasion; the second halving, however, results in the lowest value of 1.38 GWh. When (2.40) is replaced by the linear-coefficient data of (2.41) (9a-e, 11a-e, and 13a-e), we find that a smaller amount of energy is produced in each of the three cases, since the volume of the *linear* estuary is less than that of the *constant* one. The

behaviour of energy with κ is the same as before, indicating the existence of an optimal value of κ (Count, 1980; Birkett, 1985). Note that there is a very significant difference between the energy obtained from the *constant* and *linear* estuaries (14a-e and 15a-e) when the tidal period is changed to 1030.633 seconds.

In practice, the computer time used in solving Problem 2 numerically is almost unnoticeably greater than that used in solving Problem 1. The additional expense in introducing a barrier into the fluid-flow problem is therefore a negligible one.

Consider now the variation of the obtained energy (as evaluated from (3.2) using the Trapezium Rule) with the tidal amplitude, ζ of (2.35). Computational results agree sufficiently well (i.e., to within ϵ) with the theoretical result for the linearised shallow-water problem; namely,

$$E \propto \zeta^2. \tag{3.26}$$

In both Problems 1 and 2, a value of unity for λ (instead of $\frac{1}{2}$, as in (2.36)) results in the convergence of the iteration for the periodic solutions of v and η in fewer iterations; for example, in the case of the run corresponding to Figures 8a-e, this increase in the value of λ produces convergence in only 2 iterations, as opposed to 8 with $\lambda = \frac{1}{2}$ (the computer time is also significantly reduced).

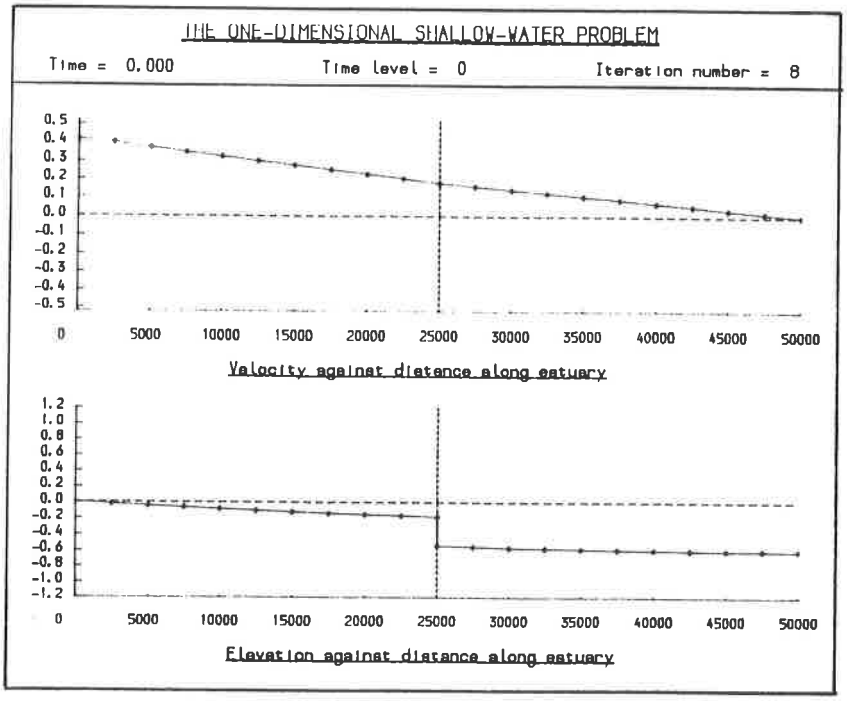

Figure 8a

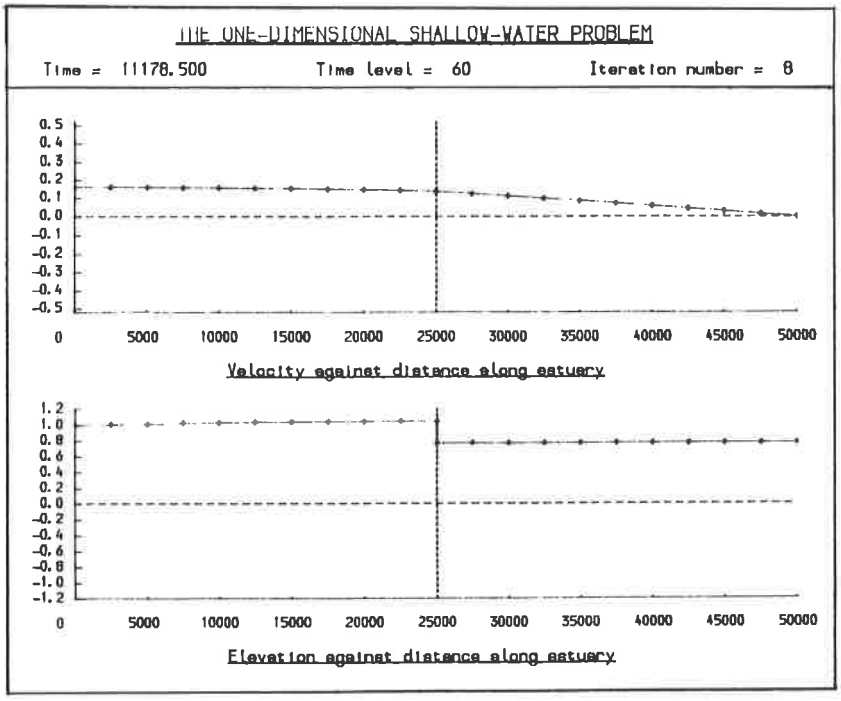

Figure 8b

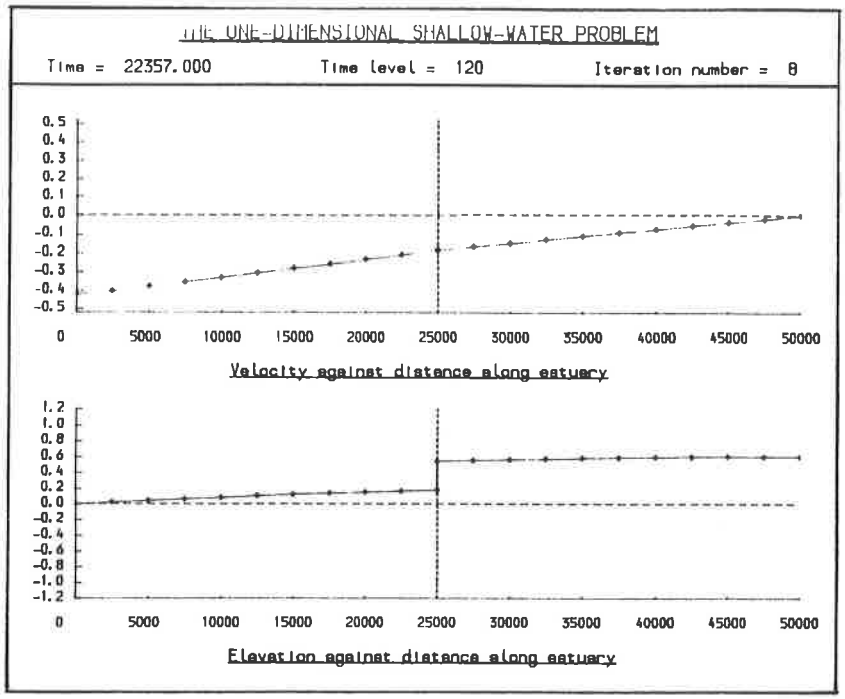

Figure 8c

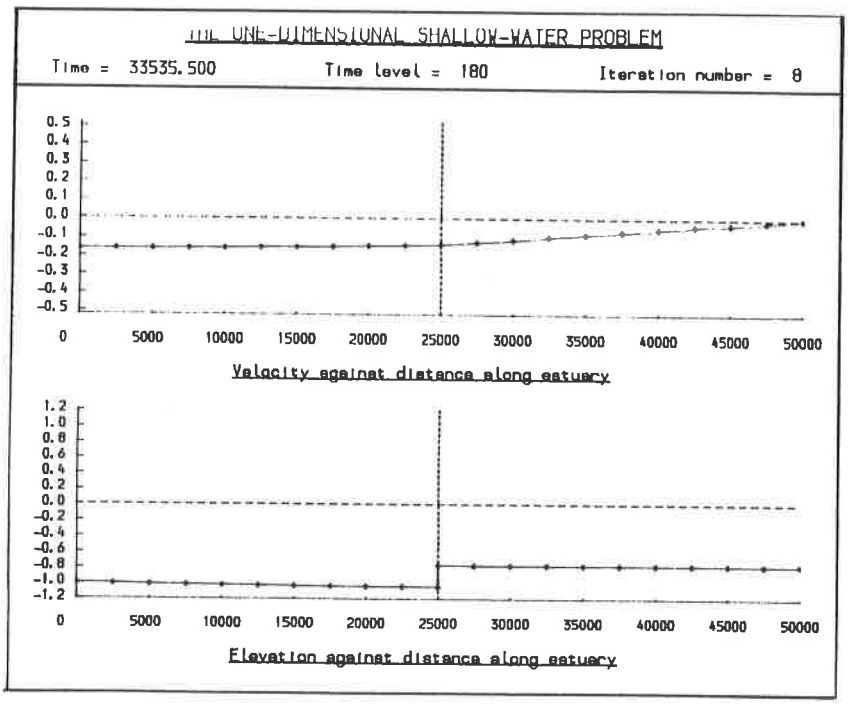

Figure 8d

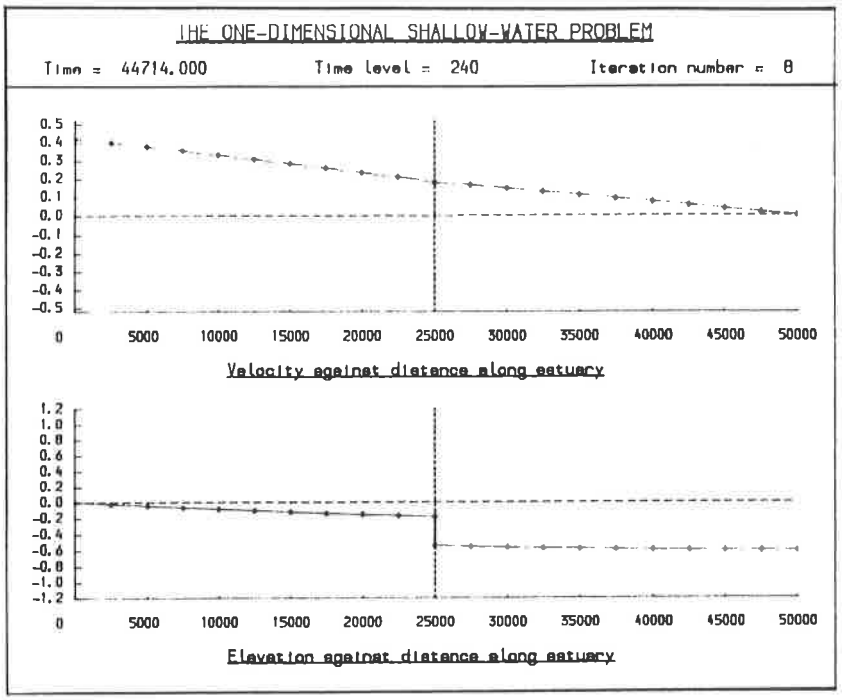

Figure 8e

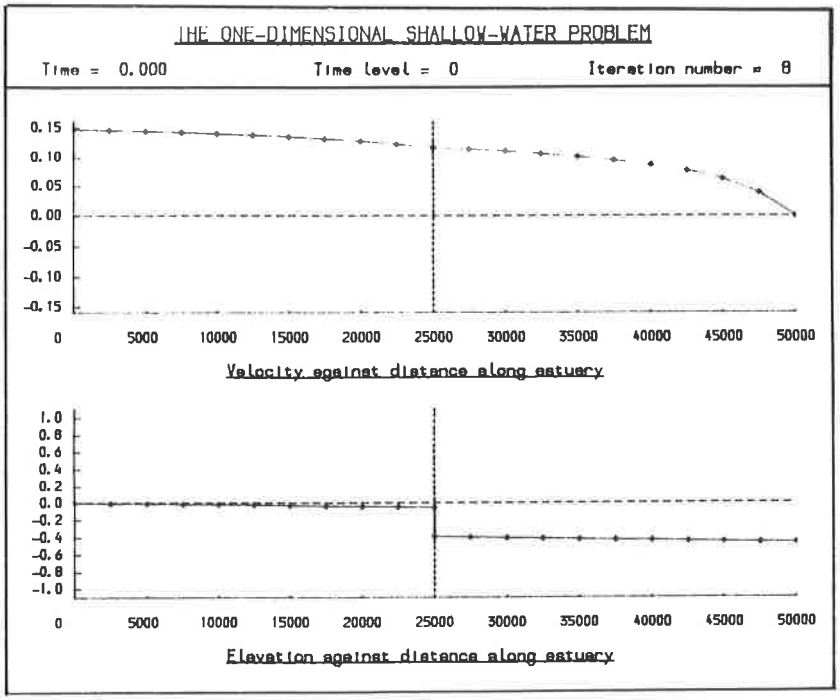

Figure 9a

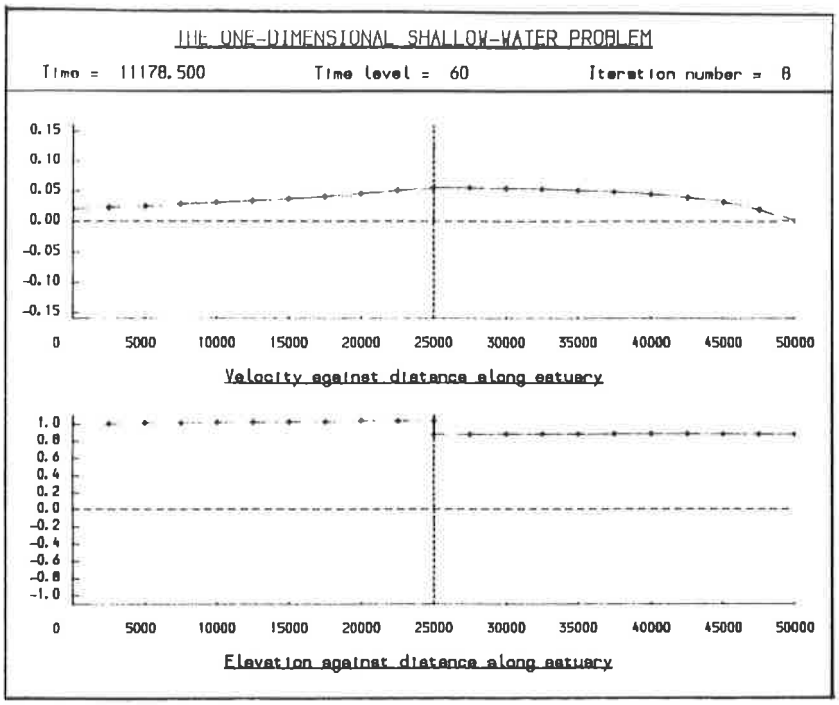

Figure 9b

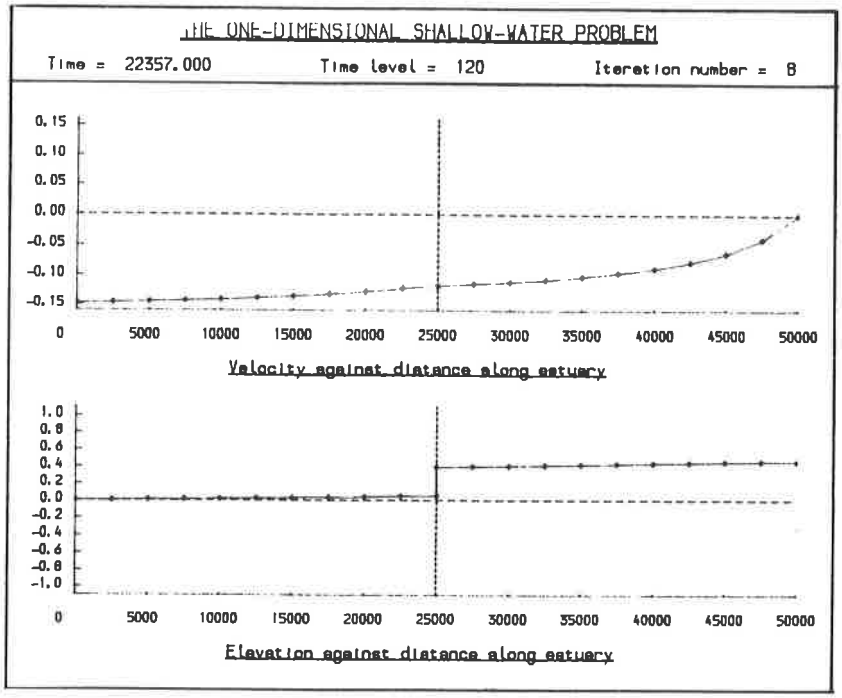

Figure 9c

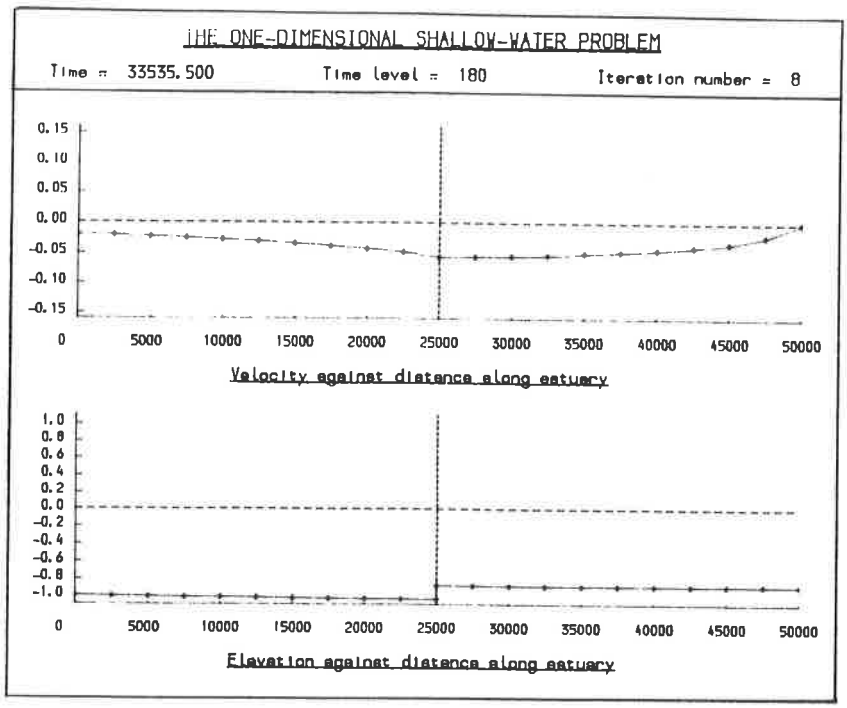

Figure 9d

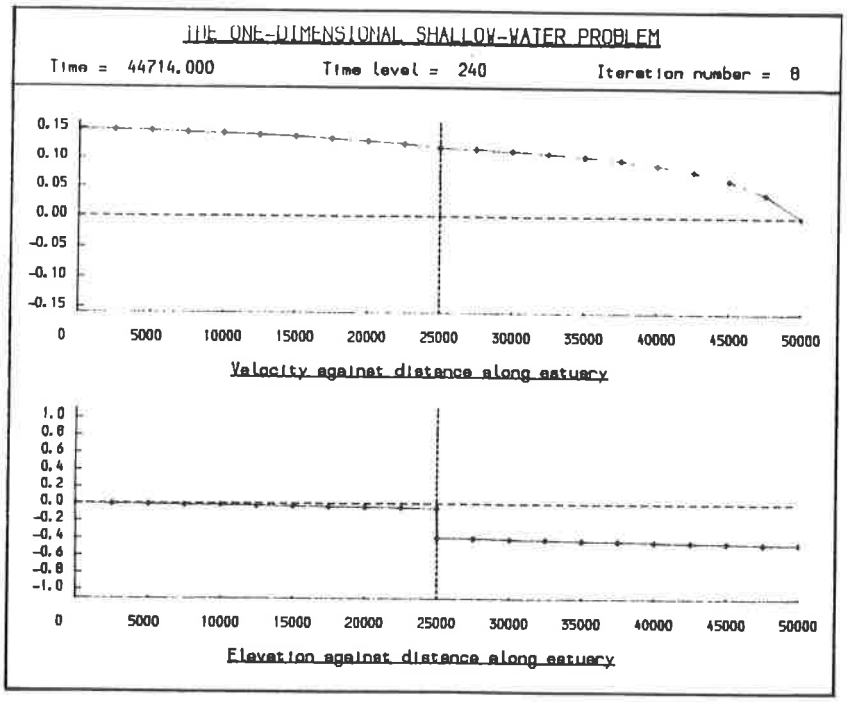

Figure 9e

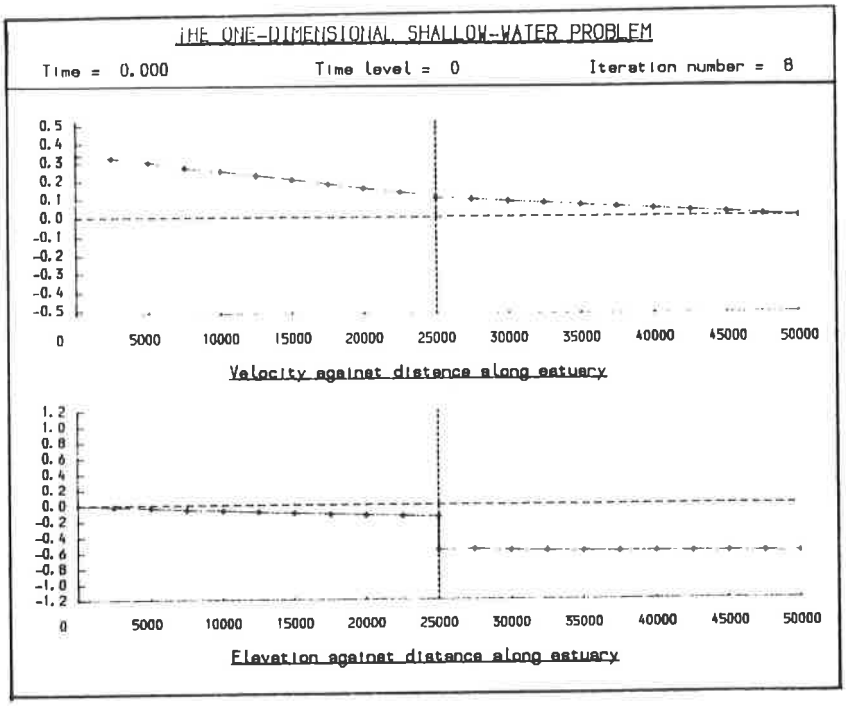

Figure 10a

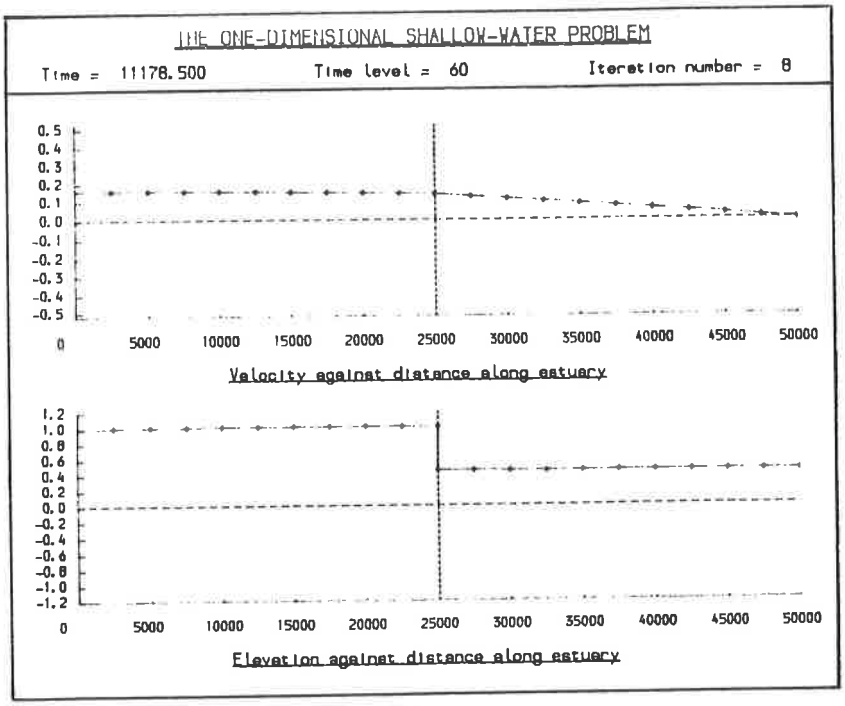

Figure 10b

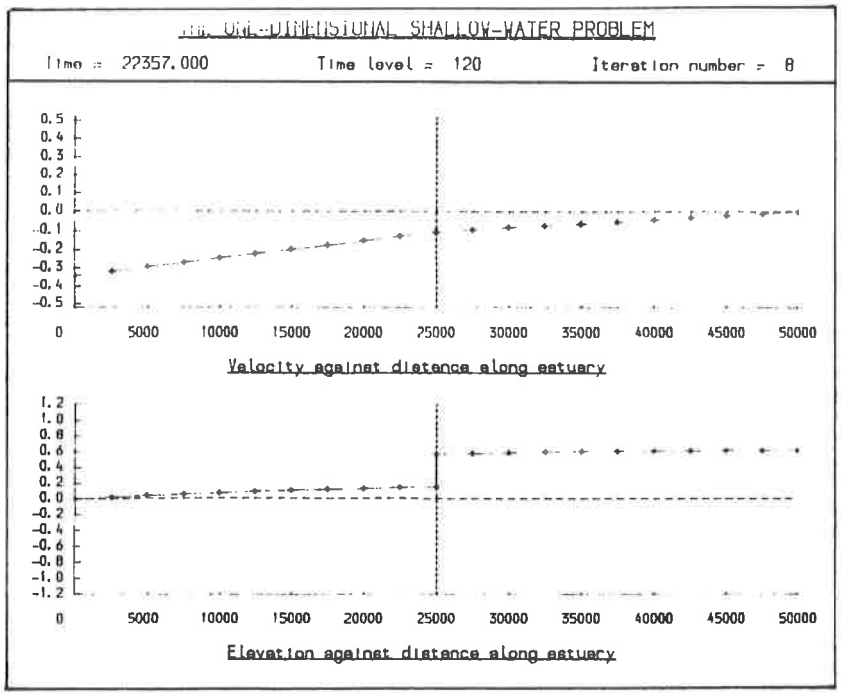

Figure 10c

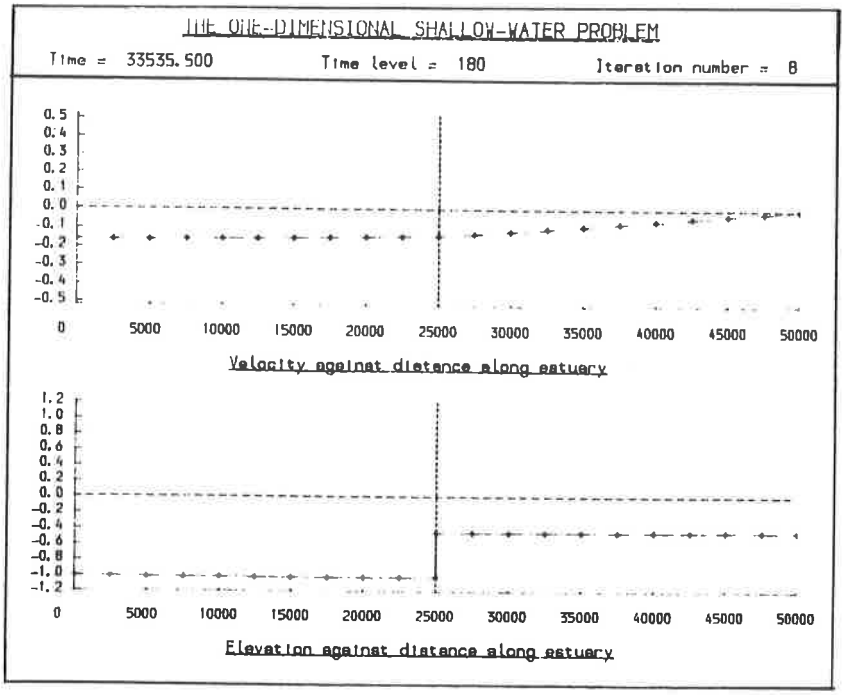

Figure 10d

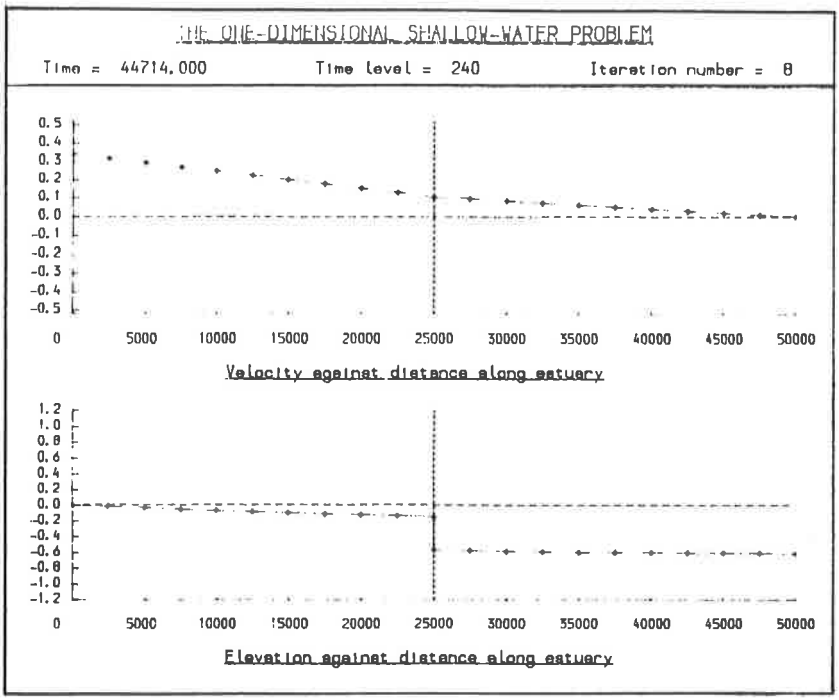

Figure 10e

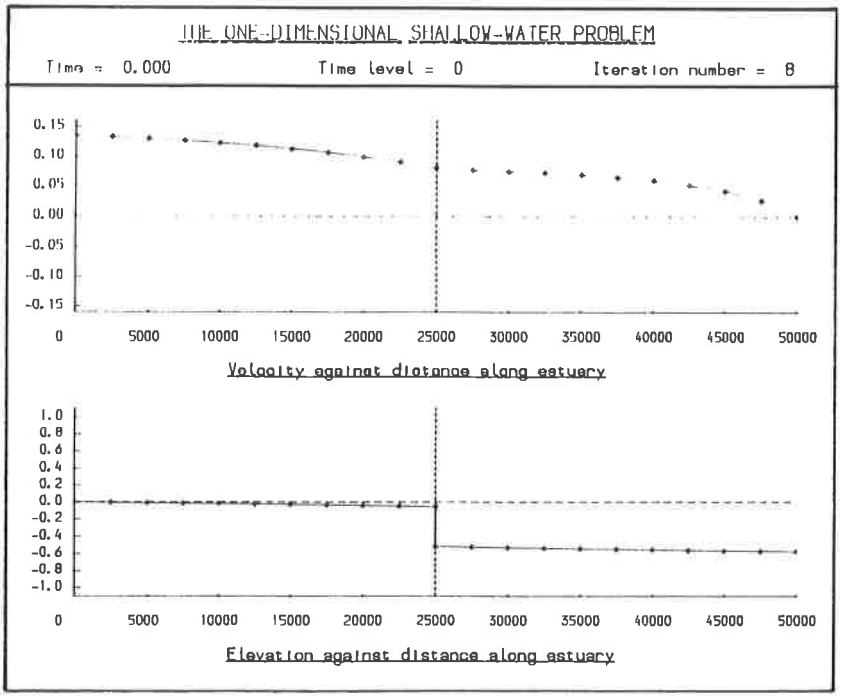

Figure 11a

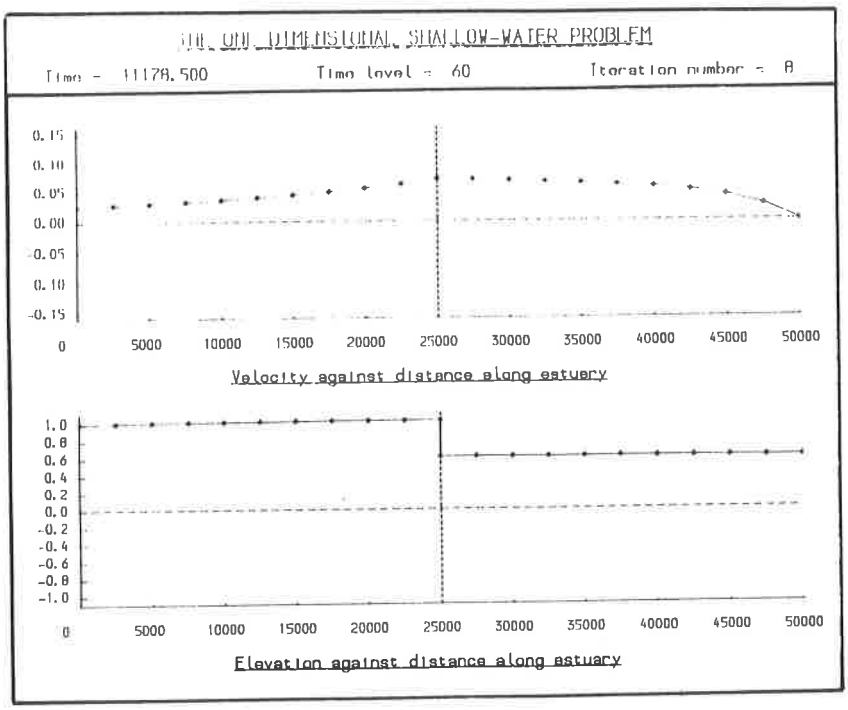

Figure 11b

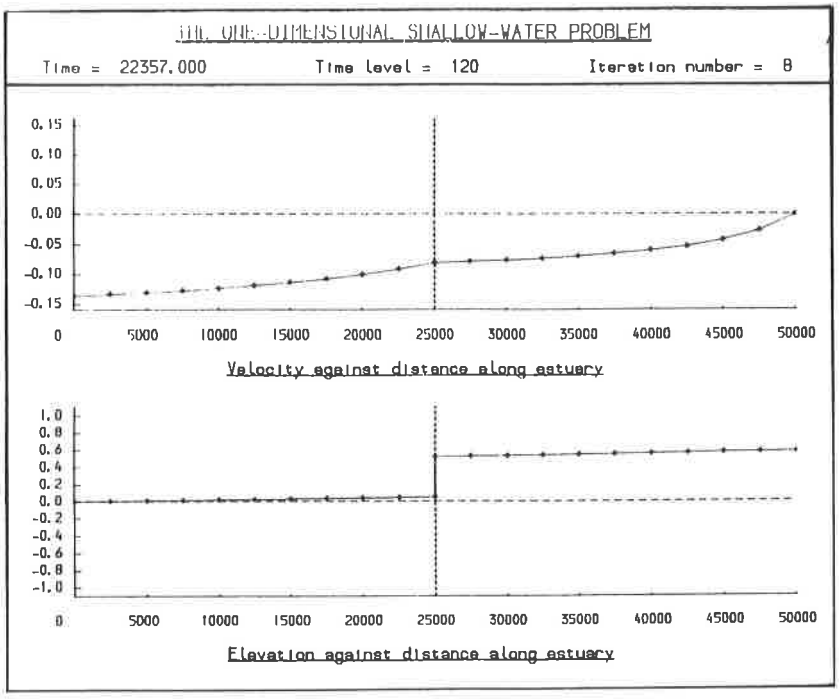

Figure 11c

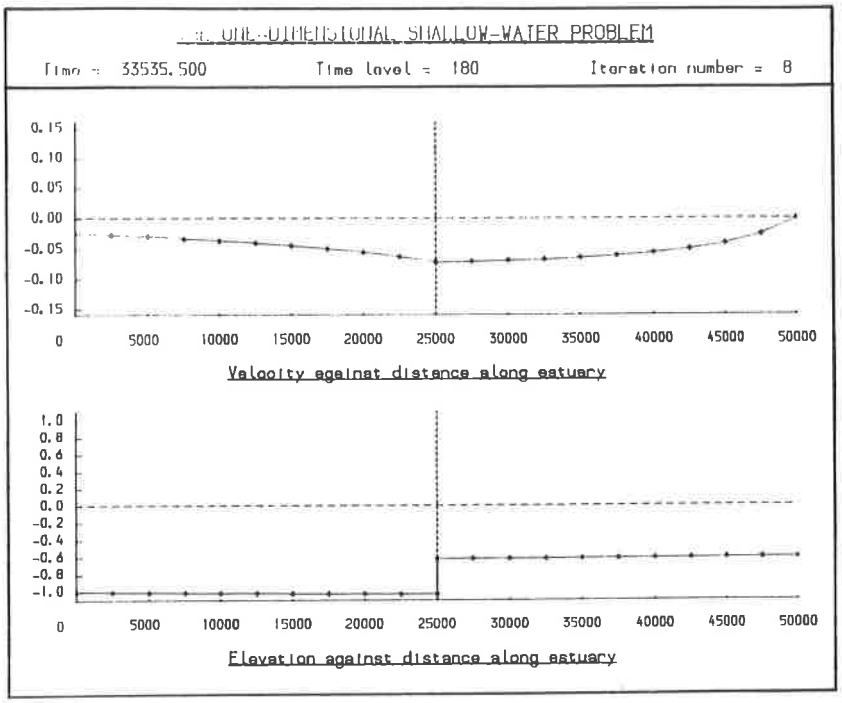

Figure 11d

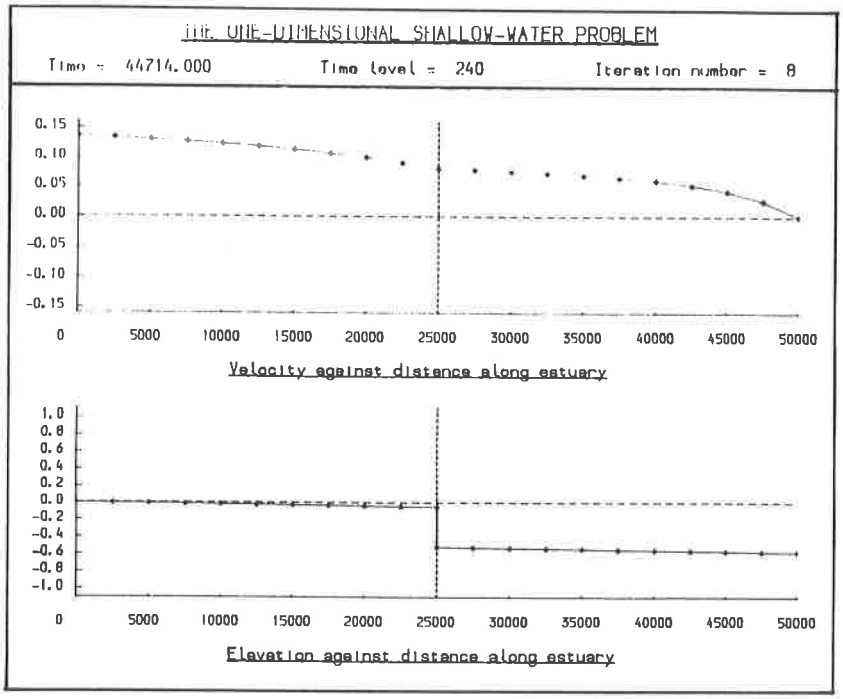

Figure 11e

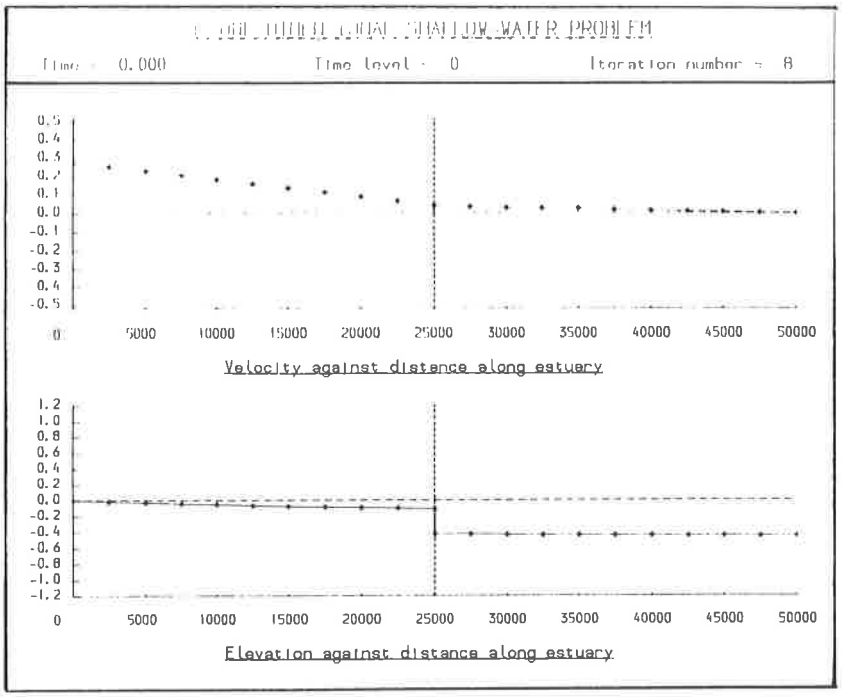

Figure 12a

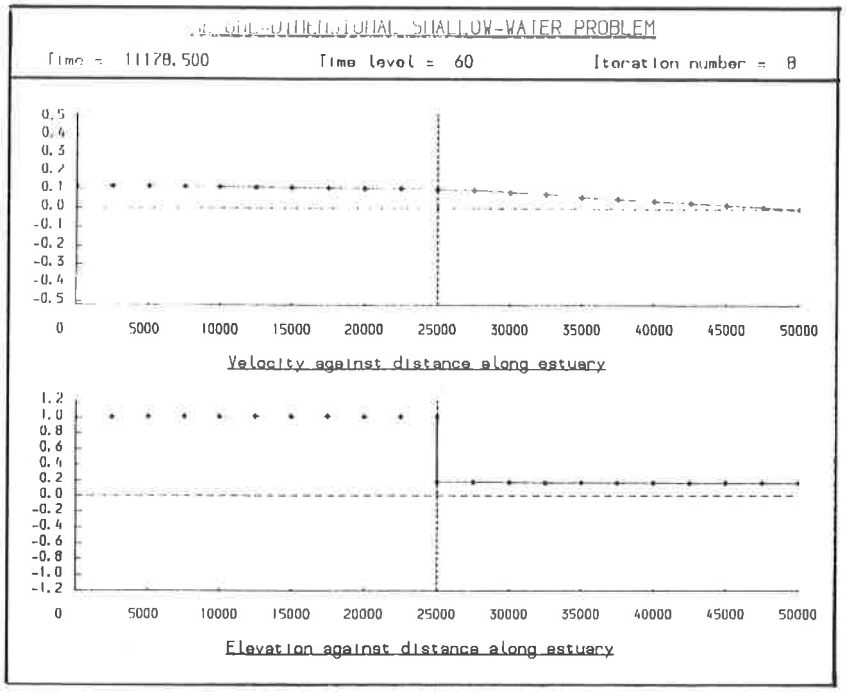

Figure 12b

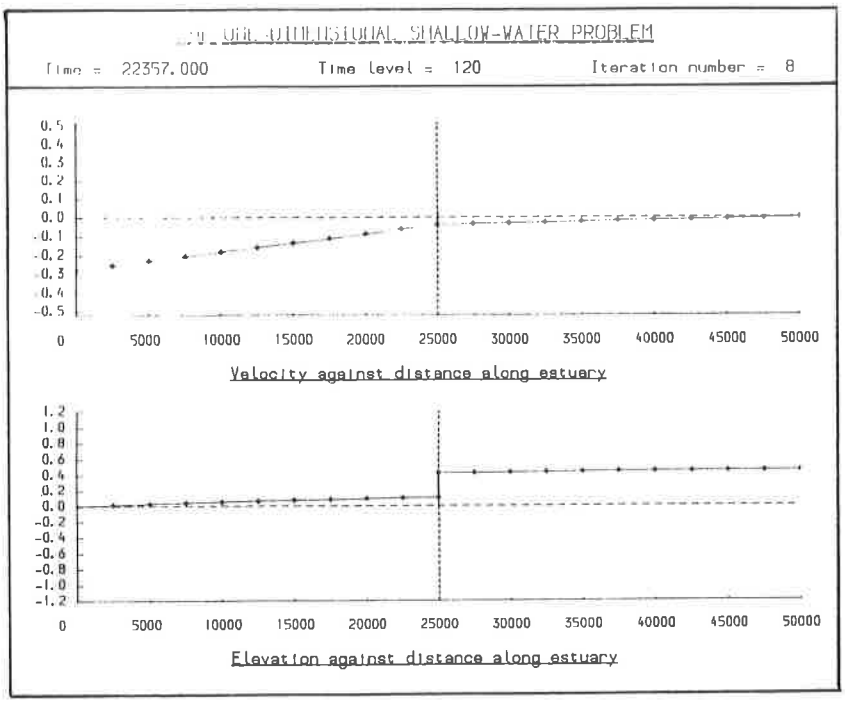

Figure 12c

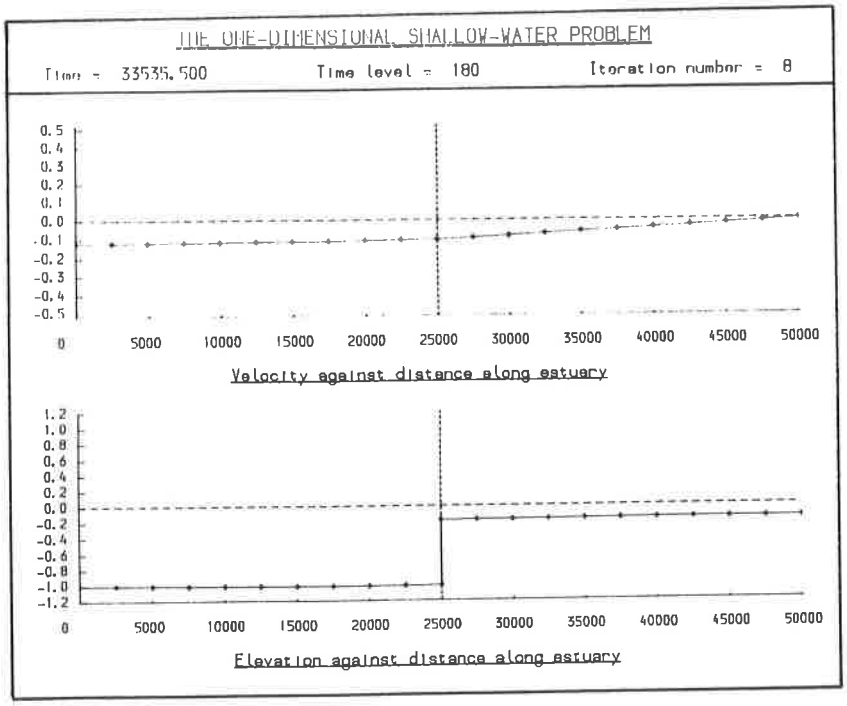

Figure 12d

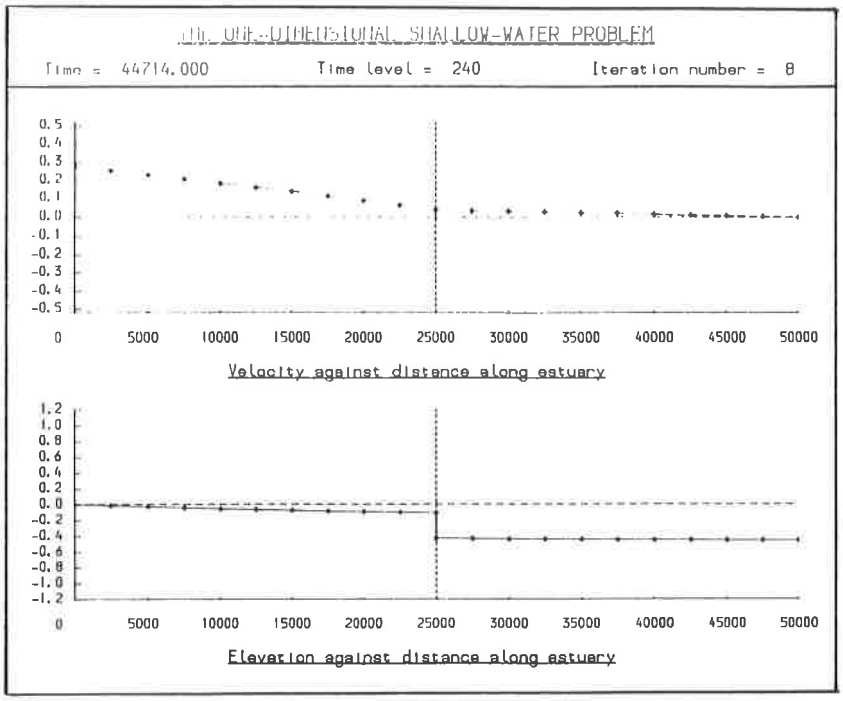

Figure 12e

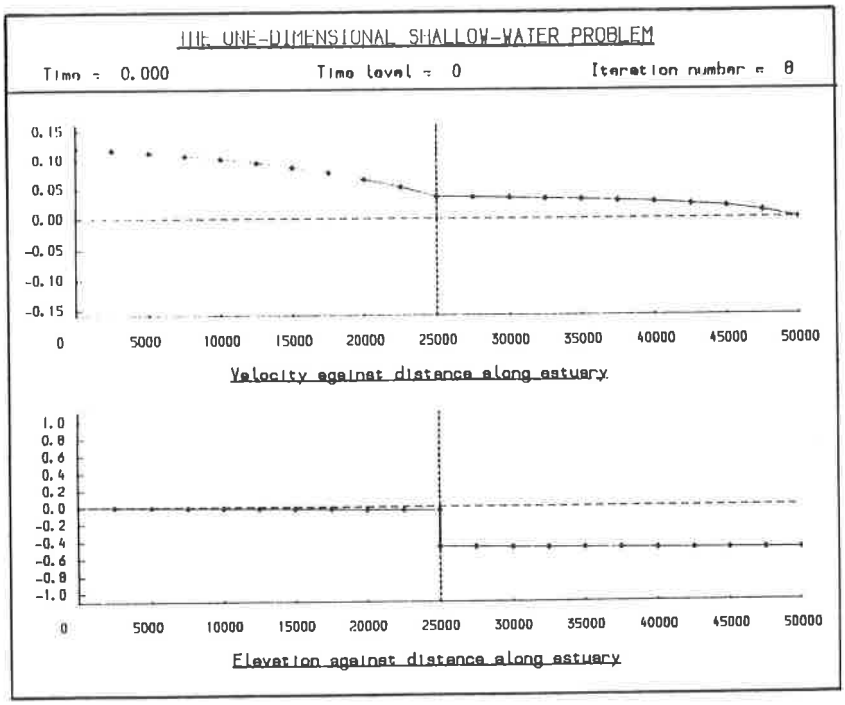

Figure 13a

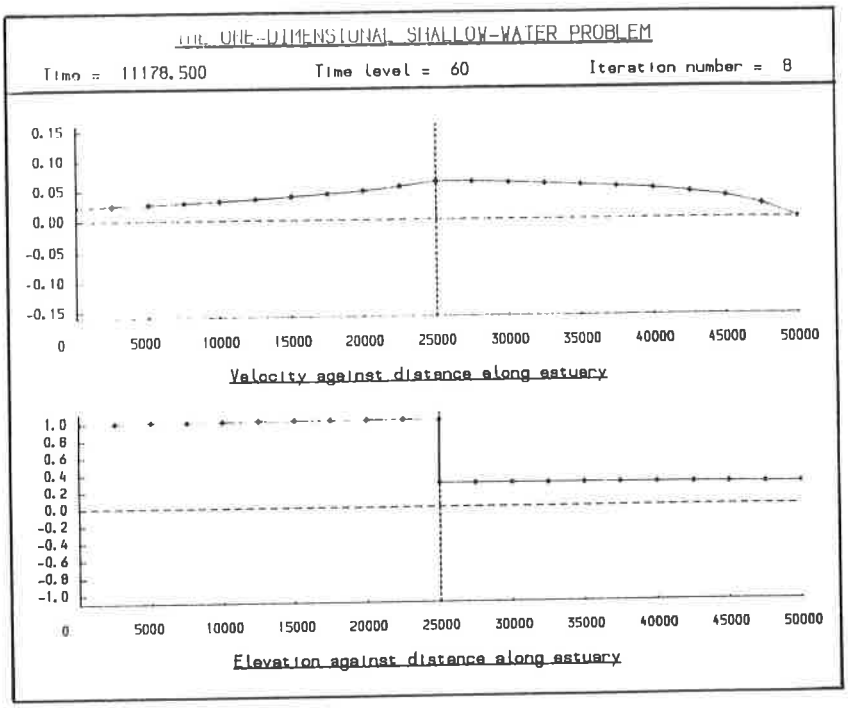

Figure 13b

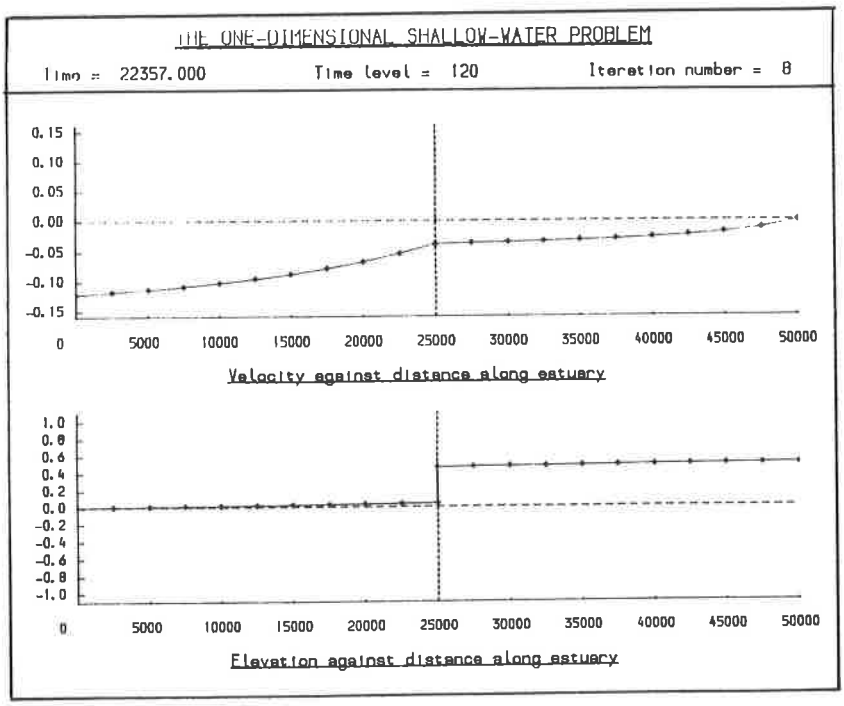

Figure 13c

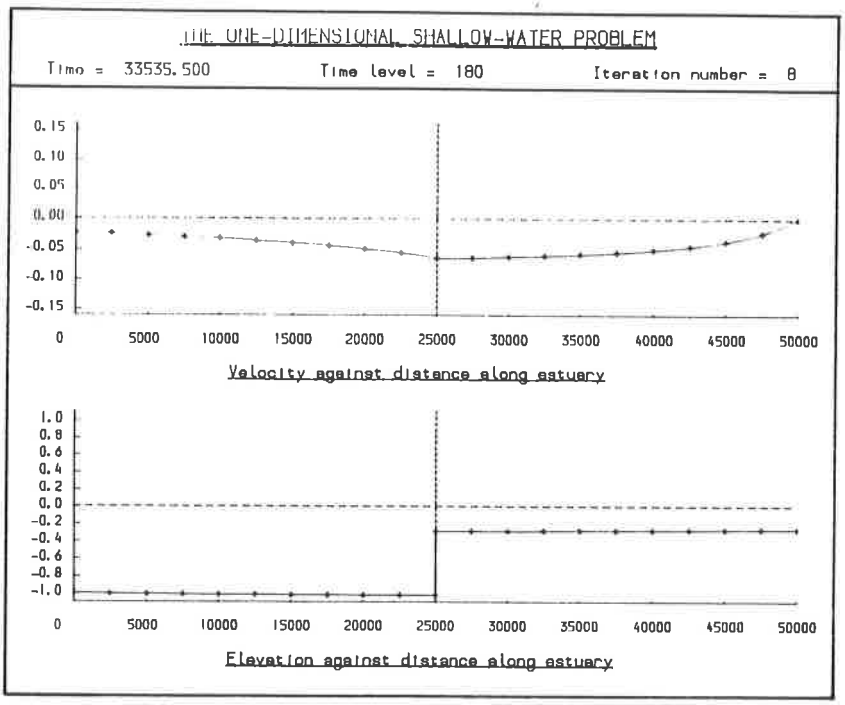

Figure 13d

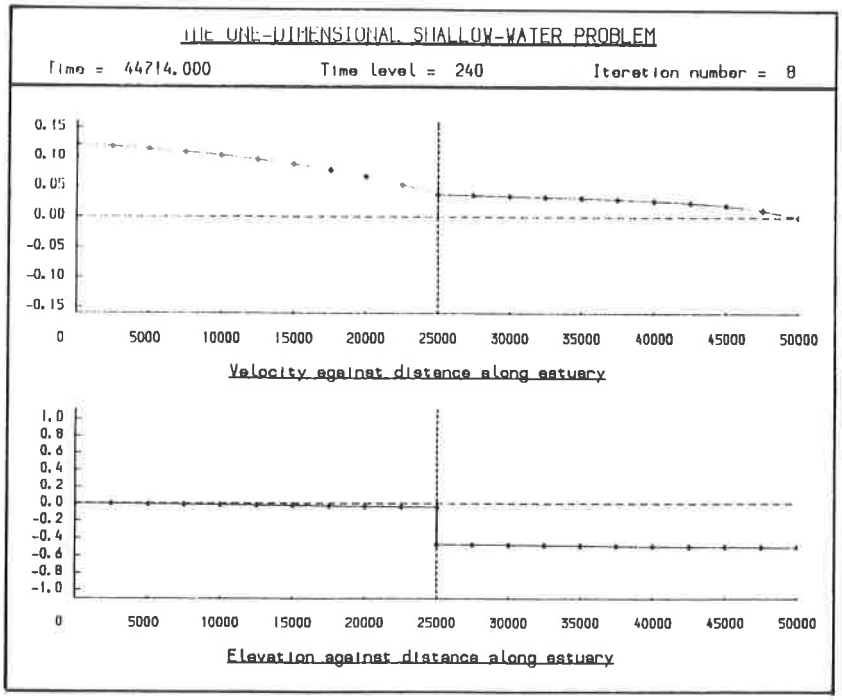

Figure 13e

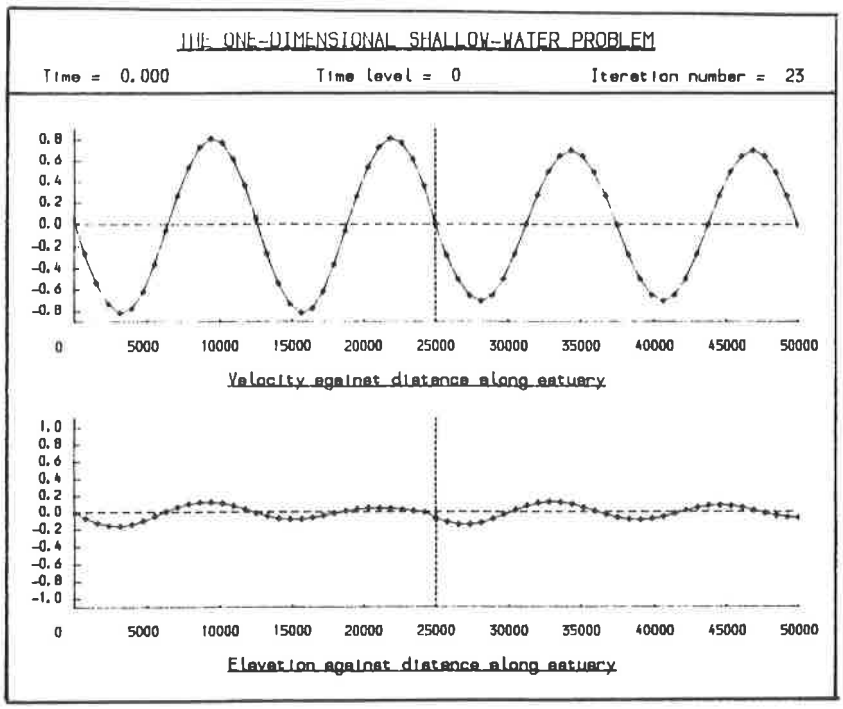

Figure 14a

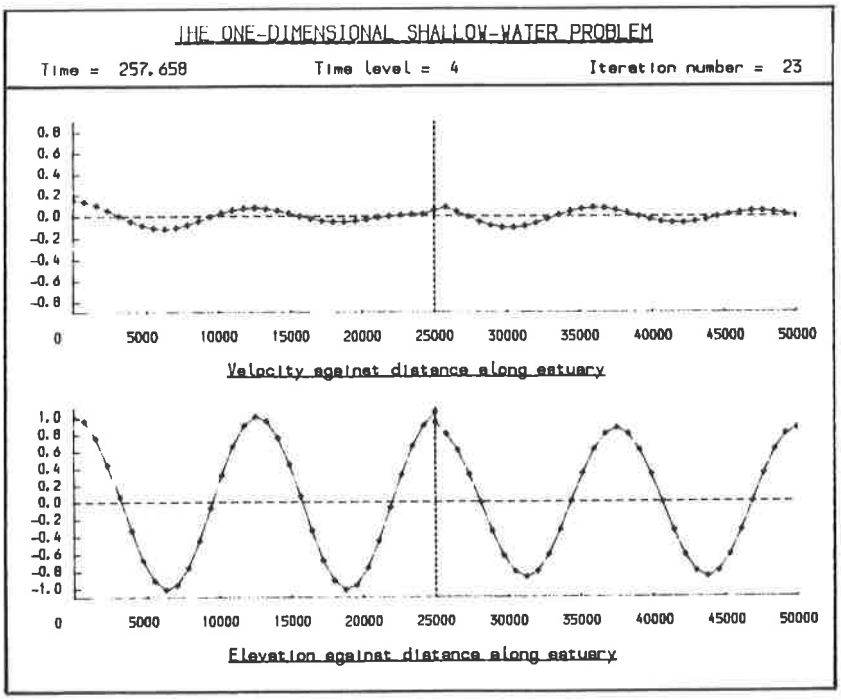

Figure 14b

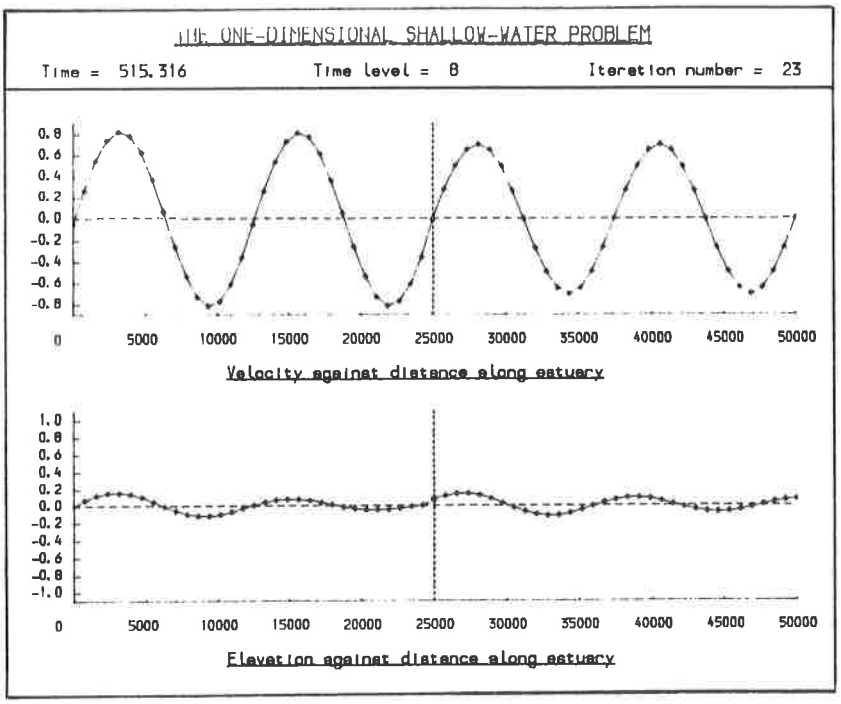

Figure 14c

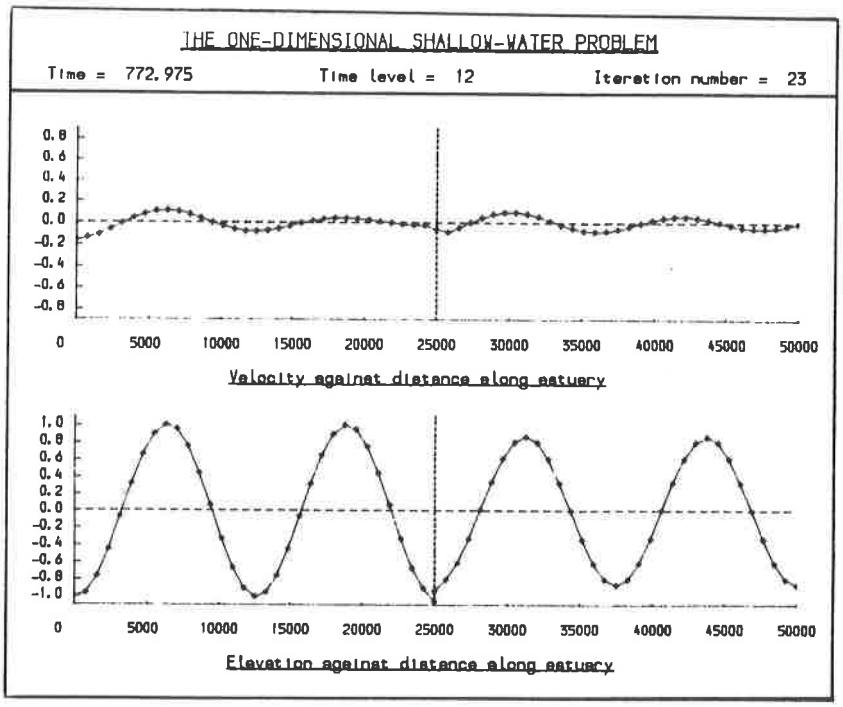

Figure 14d

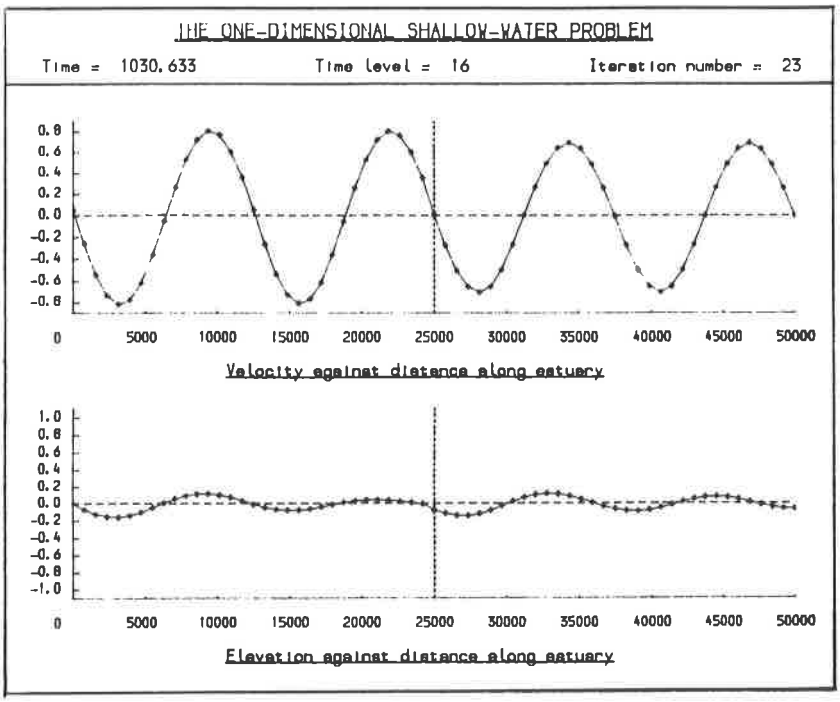

Figure 14e

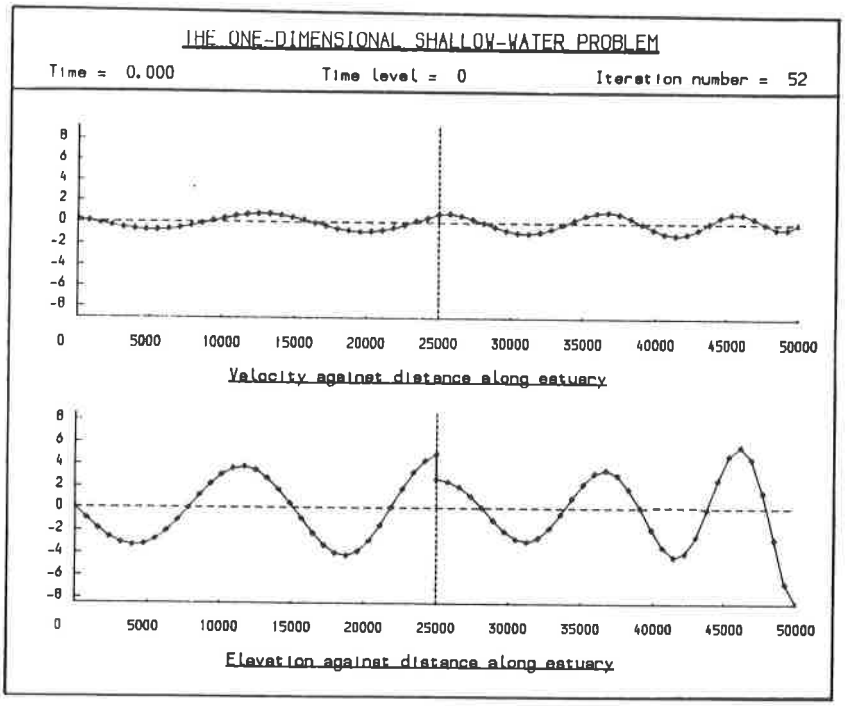

Figure 15a

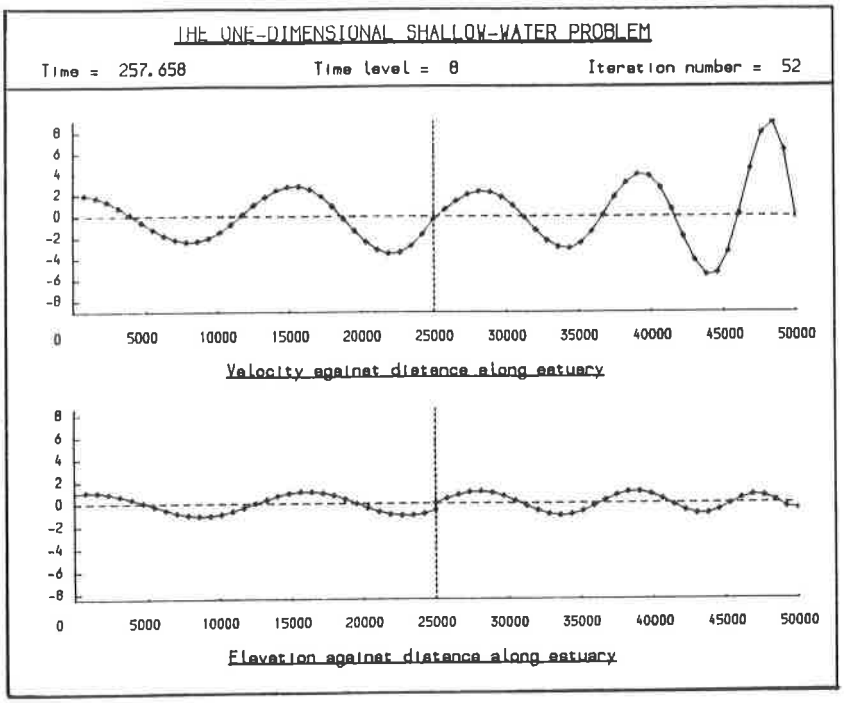

Figure 15b

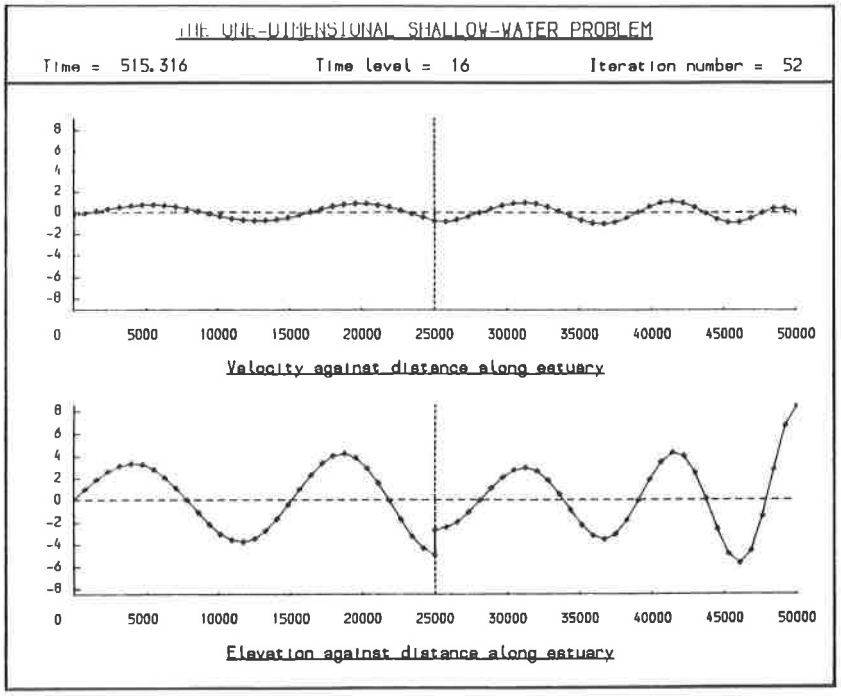

Figure 15c

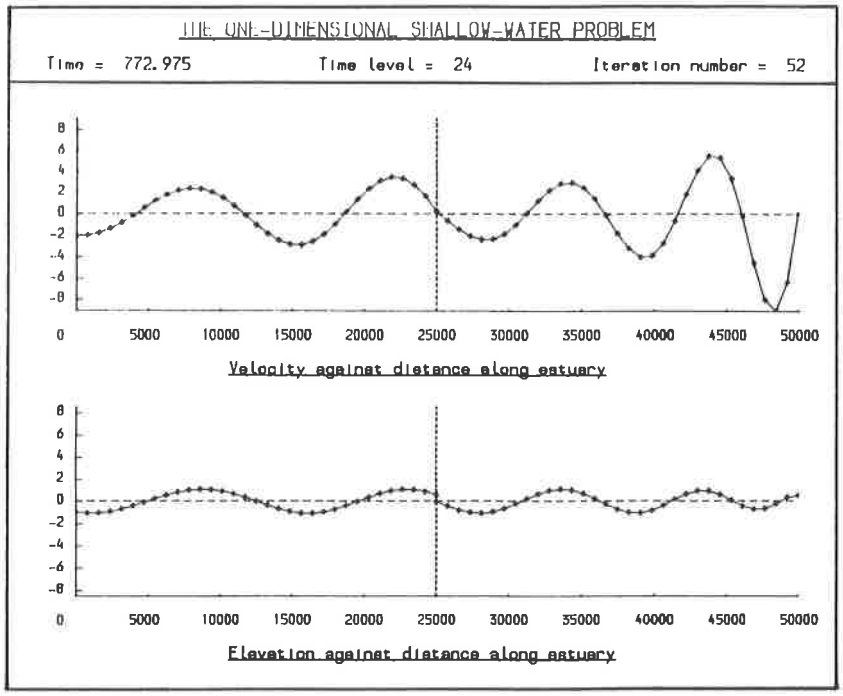

Figure 15d

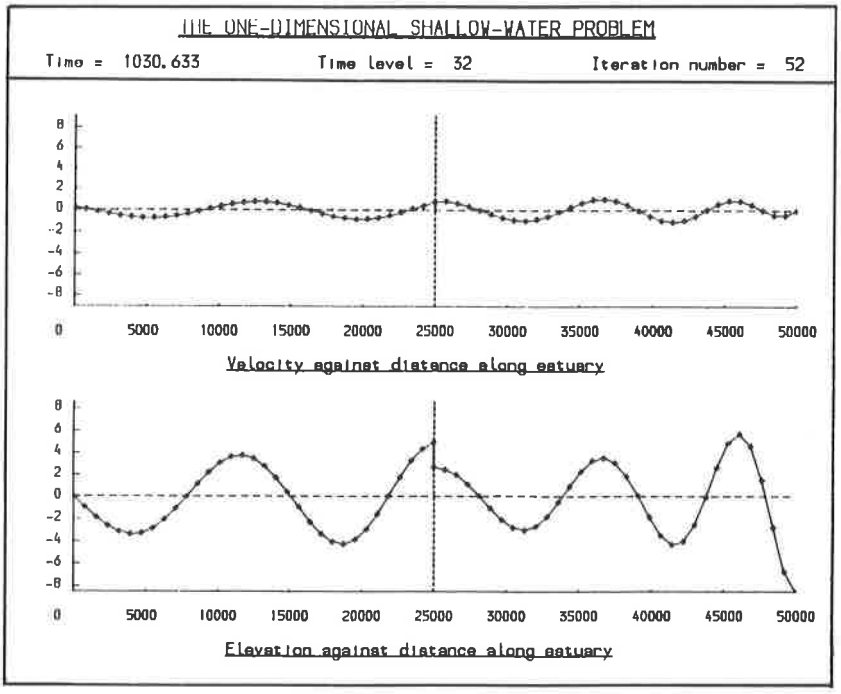

Figure 15e

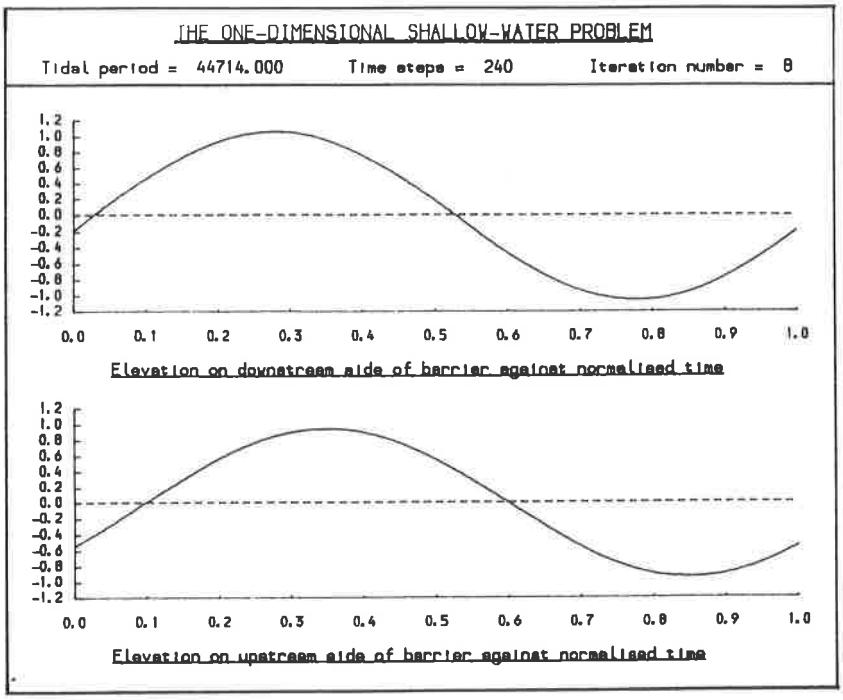
THE ONE-DIMENSIONAL SHALLOW-WATER PROBLEM
Tidal period = 44714.000
Time steps = 240
Iteration number = 8
1.2
1.0
0.8
0.6
0.4
0.2
0.0
-0.2
-0.4
-0.6
-0.8
-1.0
-1.2
0.0 0.1 0.2 0.3 0.4 0.5 0.6 0.7 0.8 0.9 1.0
Elevation on downstream side of barrier against normalised time
Elevation on upstream side of barrier against normalised time

Figure 16

Distance (km)	Exact Velocity	e_V	Exact Elevation	e_E
0	0.42121	-76	0.00000	0
5	0.37401	-83	-0.04529	17
10	0.32619	-82	-0.08639	-26
15	0.27790	-81	-0.12311	-35
20	0.22928	-80	-0.15531	-43
25^-	0.18047	-35	-0.18284	-105
25^+	0.18047	-35	-0.54381	-176
30	0.14443	5	-0.56652	-125
35	0.10836	5	-0.58427	-126
40	0.07225	3	-0.59699	-126
45	0.03613	1	-0.60464	-127
50	0.00000	0	-0.60719	-127

Table 5

Distance (km)	Exact Velocity	e_V	Exact Elevation	e_E
0	0.16082	-31	1.00000	0
5	0.15974	-26	1.01486	-10
10	0.15664	-25	1.02649	-14
15	0.15172	-23	1.03501	-18
20	0.14518	-22	1.04056	-22
25^-	0.13724	-22	1.04323	-29
25^+	0.13724	-22	0.76872	-81
30	0.11122	-23	0.76980	-45
35	0.08425	-18	0.77054	-18
40	0.05656	-12	0.77103	31
45	0.02840	-6	0.77130	32
50	0.00000	0	0.77138	32

Table 6

Data	Energy (GWh)
8a-e	1.422
9a-e	0.963
10a-e	1.688
11a-e	1.341
12a-e	1.358
13a-e	1.240
14a-e	0.002
15a-e	0.911

Table 7

4. CONCLUSIONS

In this report we presented two mathematical formulations of shallow-water problems: one without a barrier, Problem 1 (in Subsection 2.1), and one with a barrier, Problem 2 (in Subsection 3.1). We also described the Taylor-Galerkin Method (in Subsection 2.2), which we utilised to solve Problems 1 and 2. Additional numerical treatments (of Subsection 3.3) were necessary for Problem 2, for which a simple analytic solution was derived (in Subsection 3.2). Numerical results (arising from various experiments) were conducted and the outcomes were discussed in Subsections 2.3 and 3.4 for Problems 1 and 2 respectively. In the case of Problem 1, we varied the coefficient functions, tidal period, numbers of nodes and time steps, and also the C.F.L. number, obtaining a wide selection of velocity and elevation graphs. On analysing the accuracy of the method, we discovered an order of approximately two (a value below that established by Donea (1984)). The linearity of the velocity and elevation with the tidal amplitude was also observed. On introducing a barrier (to produce Problem 2), we observed that (i) both v_x and η were discontinuous across the barrier, the extent of which depended on κ, (ii) the Taylor-Galerkin Method was not as accurate for this problem (as a consequence of (3.1), and possibly its discretisation via (3.19) and (3.20)), and (iii) the energy obtained from the generation scheme varied according to the square of the tidal amplitude (see (3.26)).

The computer times for the Taylor-Galerkin Method on Problems 1 and 2 were reasonably high, indicating a fairly expensive solution technique;

the times consumed in solving Problem 2 were negligibly different from those for Problem 1). The numerical results, however, were extremely accurate.

A future task is to introduce a nonlinear relationship at the barrier (in place of (3.1)) into Problem 2. Such a relationship will involve the functions describing the flow through the turbines and sluices (against the head difference), P and R, say. It may also be necessary to replace the linearised shallow-water equations, (2.1), by corresponding nonlinear ones. This last operation would, however, require considerably more algebra in order to arrive at modified forms of (2.15) and (2.16). The amount of algebra necessary to facilitate an extension of the Taylor-Galerkin Method to a fully nonlinear problem in two space dimensions would be immense. The large number of necessary algebraic manipulations is the drawback of the method, which is ideal for simple problems.

The next ammendment to Problem 2 is the introduction of an optimal-control loop. Such a loop should have the property that derivatives, such as P' and R', are not required in the algorithm (Moody, 1989). After the successful completion of this task, the next would be one of the more complicated ones of the previous paragraph.

ACKNOWLEDGEMENTS

I would like to thank Dr. Mike Baines (in the absence of my supervisor, Dr. Nancy Nichols) for his continuous interest in, and for his helpful suggestions concerning, this project. I also acknowledge Dr. Nick Birkett for his technical advice.

REFERENCES

BERRY, P.E. 1982 "On the Use of the Describing Function Technique for Estimating Power Output from a Tidal Barrage Scheme", *Technical Report TPRD/M/1292/N82 TF425*, Marchwood Engineering Laboratories, CEGB.

BERRY, P.E., BIRKETT, N.R.C., COUNT, B.M., & NICOL, D.A.C. 1984 "Optimal Control Theory Applied to Tidal Power", *IEE Conference Publication Number* 233, Fourth International Conference on Energy Options.

BIRKETT, N.R.C. 1985 *Optimal Control in Tidal Power Calculations*, Ph.D. Thesis, Department of Mathematics, University of Reading.

BIRKETT, N.R.C. 1986 "Non-linear Optimal Control of Tidal Power Schemes in Long Estuaries", *Numerical Analysis Report* 9/86, Department of Mathematics, University of Reading.

BIRKETT, N.R.C. 1989 Private communication.

BIRKETT, N.R.C., COUNT, B.M., & NICHOLS, N.K. 1984 "Optimal Control Problems in Tidal Power", *Journal of Dam Construction and Water Power*, pp. 37-42.

BIRKETT, N.R.C., COUNT, B.M., NICHOLS, N.K., & NICOL, D.A.C. 1984 "Optimal Control Problems in Tidal Power Generation", *Applied Optimisation Techniques in Energy Problems* (Ed. H. Wacker), B.G. Teuber, Stuttgart,

pp. 138-159.

BIRKETT, N.R.C., & NICHOLS, N.K. 1983 "The General Linear Problem of Tidal Power Generation with Non-linear Headflow Relations", *Numerical Analysis Report* 3/83, Department of Mathematics, University of Reading.

BIRKETT, N.R.C., & NICHOLS, N.K. 1986 "Optimal Control Problems in Tidal Power", in *Industrial Numerical Analysis* (Eds. S. McKee & C.M. Elliot), Clarendon Press, Oxford.

COUNT, B.M. 1980 "Tidal Power Studies at M.E.L.", *Technical Report MM/MECH/TF257*, Marchwood Engineering Laboratories, CEGB.

DONEA, J. 1984 "A Taylor-Galerkin Method for Convective Transport Problems", *Int. J. Numer. Meth. Engrg.* 20, pp. 101-119.

H.M.S.O. 1981 "Tidal Power from the Severn Estuary", *Energy Paper Number* 46.

JEFFERYS, E.R. 1981 "Dynamic Models of Tidal Estuaries", Proceedings of BHRA Second International Conference on Wave and Tidal Energy.

MOODY, R.O. 1989 "The Application of Optimal Control Theory to Tidal-power-generation Problems", *Numerical Analysis Report* 7/89, Department of Mathematics, University of Reading.

WILSON, E.M., *ET AL.* 1981 "Tidal Energy Computations and Turbine

Specifications", Institute of Civil Engineers Symposium on the Severn Barrage.